Spatio-temporal structure of Baltic free sea level oscillations in barotropic and baroclinic conditions from hydrodynamic modelling.

Eugeny A. Zakharchuk[1,2], Natalia Tikhonova[1,2], Elena Zakharova[3,4]

[1]Saint-Petersburg University, Saint-Petersburg, 199004, Russia
[2] State Oceanographic Institute. Saint-Petersburg Branch, Saint-Petersburg, 199397, Russia
[3]Water Problem Institute, RAS, Moscow, 117971, Russia
[4]EOLA, Toulouse, 31400, France

Correspondence to: Elena Zakharova (zavocado@gmail.com)

Abstract. Free sea level oscillations in barotropic and baroclinic conditions were examined using numerical experiments based on a 3D hydrodynamic model of the Baltic Sea. In a barotropic environment, the highest amplitudes of free sea level oscillations are observed in the northern Gulf of Bothnia, eastern Gulf of Finland, and south-western Baltic Sea. In these areas, the maximum variance appears within the frequency range corresponding to periods of 13–44 hr. In a stratified environment, after the cessation of meteorological forcing, water masses relax to the equilibrium state in the form of mesoscale oscillations at the same frequencies as well as in the form of rapidly decaying low-frequency (seasonal) oscillations. The total amplitudes of free baroclinic perturbations are significantly larger than those of barotropic perturbations, reaching 15–17 cm. Contrary to barotropic, oscillations in baroclinic conditions are strongly pronounced in the deep-water areas of the Baltic Sea proper. Specific spatial patterns of amplitudes and phases of free barotropic and baroclinic sea level oscillations identified them as progressive-standing waves representing barotropic or baroclinic modes of gravity waves and topographic Rossby waves.

1 Introduction

The Baltic Sea level perturbations represent a superposition of free and forced oscillations of different spatial and temporal scales. These oscillations can be generated either within the Baltic basin or come from the North Sea via the narrow and shallow Danish Straits (Samuelsson and Stigebrandt, 1996). The Baltic Sea water masses experience continuous effect of external and internal forces related to tides, wind stress, atmospheric pressure, changes of water density or of water balance constituents. After cessation of the perturbing forces, the water masses return to equilibrium in form of barotropic or baroclinic modes of free oscillations, rapidly attenuated by dissipative forces (Leppäranta and Myrberg, 2009; Proshutinsky, 1993; Zakharchuk et al., 2004).

Free sea level oscillations are directly related to the eigenoscillations of sea basins. The spectral structure of eigenoscillations depends on sea basin scales, basin bathymetry, and land configuration. In eigenoscillation frequencies, the basin water masses return to equilibrium conditions after meteorological forcing (Fennel and Seifert, 2008; Leppäranta and Myrberg, 2009; Lisitzin, 1974). Within these frequencies, the free oscillations may resonate with wind forcing, resulting in an anomalous sea level rise followed by the inundation of coastal areas (Jönsson et al., 2008; Zakharchuk and Tikhonova, 2011). The investigation into free oscillations of sea basins is

essential for correctly interpreting the spatio-temporal variability of physical, hydrochemical, and biological parameters, as well as for identifying the mechanisms responsible for this variability.

The Baltic Sea free oscillations are usually related to seiches. Seiches are free sea level fluctuations in an enclosed or semi-isolated basin, which occur as standing waves generated by external forcing and continue due to inertia after cessation of the initial force (Lisitzin, 1959; Proudman, 1953; Pugh, 1987). Previous studies based on spectral analysis of the Baltic Sea tide gauge records have described several Baltic seiche systems. One system is located on the West Baltic–Gulf of Finland axis and is characterised by periods of 26–32 h in the primary mode and 17–20 h in the secondary mode (Kulikov and Medvedev, 2013; Lisitzin, 1959; Magaard and Krauss, 1966; Neumann, 1941). The primary mode of the second rapidly damping seiche system situated in the Western Baltic- the Bothnia Bay axis, has a 39 h period (Neumann, 1941).

Using a one-dimensional simplified numeric model, on the axis the Gulf of Finland–Danish Straits, Neumann (1941) detected seiches with a 27-h period. The amplitude of these seiches was usually less than 10 cm, rarely reaching 40 cm. Nevertheless, higher amplitudes were not excluded.

(Metzner et al., 2000) demonstrated that the Baltic free sea-level oscillations can be studied using satellite altimetry combined with numerical modelling and in situ observations.

Research on free sea level oscillations based on numerical modelling found a more complex system of seiches in the Baltic Sea. Using a two-dimensional shallow water model with 10 km spatial resolution, Wübber and Krauss (Wübber and Krauss, 1979) suggested ten modes of the Baltic Sea eigenoscillations. The first four modes have periods of 31, 26, 22, and 20 h, respectively. The authors noted that the eigenoscillations were significantly modified by the Coriolis force. Earth's rotation transforms all modes of eigenoscillations to positive amphidromic waves. As a result, the period of oscillations may diminish (if this period is higher than an inertial period) or may increase (if it is lower than the inertial period).

Subsequently, Jönsson (Jönsson et al., 2008), based on the analysis of linear shallow-water model simulations, identified three different local oscillatory modes: in the Gulf of Finland (with two 23 and 27 h periods), Danish Belt Sea (with periods of 23–27 h), and Gulf of Riga (with 17 h periods). The authors attributed these variations to seiches and noted that they were not connected to each other. However, this conclusion is not convincing, as it was not supported by the spatio-temporal distribution of the oscillation phases. The authors also suggested that the Baltic free sea level oscillations can be related to Kelvin waves that propagate from the Gulf of Finland into the Baltic proper along the coastline.

Another study (Zakharchuk et al., 2004) that was based on simulation results of a hydrodynamic three-dimensional model implies that low-frequency free oscillations in the Baltic Sea represent the topographic Rossby waves because their phase velocity is significantly lower than that of the barotropic gravity waves.

All previous studies based on numerical modelling investigated only the barotropic variations in the Baltic sea level, while an actual sea basin is a baroclinic system. The specifics of the relaxation of the Baltic Sea water masses to equilibrium after the cessation of meteorological forces in baroclinic conditions remain unclear.

The present study investigates the difference between barotropic and baroclinic free sea level oscillations in the Baltic Sea using a three-dimensional hydrodynamic model. First, the capability of the model to simulate sea level fluctuations in different parts of the Baltic Sea was verified against in situ tide gauge observations (Section 2.3). Then, the spatio-temporal structure of the sea level variations in barotropic (Section 3.1) and baroclinic (Section 3.2) conditions is analysed using Fourier analyses of the model outputs. To interpret the detected free-

79 sea level oscillations we compared the estimated phase speed of the modelled oscillations with the theoretical
80 phase speed values of barotropic and baroclinic gravity waves and discuss the results in Section 4.
81
82 **2 Data and methods**
83
84 A three-dimensional non-linear baroclinic model developed by the Institute of Numerical Mathematics of the
85 Russian Academy of Science (Institute of Numerical Mathematics Ocean Model or INMOM) was selected for
86 studying the Baltic free sea level oscillations (Diansky et al., 2006; Zalesny et al., 2012). The model was
87 configured for the Baltic Sea basin and run in its basic setup to ensure the credibility of the sea level simulations.
88 Then, the model was re-configured for two numerical experiments to represent the barotropic and baroclinic
89 conditions in the Baltic Sea.
90
91 **2.1 Model description**
92
93 The INMOM is based on primitive equations of ocean hydrodynamics in spherical coordinates and on
94 hydrostatic and Boussinesq approximations. A dimensionless value σ is used as the vertical coordinate, which is
95 specified as $\sigma = (z - \zeta)/(H - \zeta)$, where z is the vertical coordinate; $\zeta = \zeta(\lambda, \varphi, t)$ – is the deviation of
96 the sea surface height (SSH) from the undisturbed surface as a function of longitude λ, latitude ϕ, and time t; and
97 $H = H(\lambda, \varphi)$ is the sea depth (Diansky, 2013). The prognostic variables of the model are the horizontal
98 components of the velocity vector, potential temperature T, salinity S, and deviation of sea surface height from
99 undisturbed surface. The equation of state specially designed for the numerical models is used to calculate the
100 water density (Brydon et al., 1999).
101 The INMOM includes a sea ice module that takes into account the dynamics of the sea ice, ice melting, and
102 formation of sea ice and snow, as well as the transformation of old snow to sea ice (Yakovlev, 2009). This
103 module calculates the ice drift velocity, which depends on wind, sea currents, Earth's rotation, sea surface slope,
104 and ice floe interactions described by elastic-viscous-plastic rheology (Briegleb et al., 2004). The ice module
105 uses a monotonic transfer scheme (Hunke and Dukowicz, 1997), ensuring non-negative values of ice/snow
106 concentrations and mass. Detailed description of the basic configuration of the INMOM model can be found in
107 (Moshonkin et al., 2018).
108 The INMOM has been widely used in studies of the Black and Azov Seas (Fomin and Diansky, 2018;
109 Korshenko et al., 2019; Zalesny et al., 2012), the Norwegian Sea (Morozov et al., 2019), the Barents Sea
110 (Diansky et al., 2019), and the Sea of Okhotsk (Diansky et al., 2020). For this study, the INMOM model was run
111 for two years (2009–2010) within the region bounds of 9.4°E–30.4°E and 53.6°N–65.9°N with a spatial
112 resolution of 2 nautical miles (3.7 km) in the horizontal direction, non-uniform 35 sigma-levels in the vertical
113 direction, and a 2.5-min calculation step. The model outputs represent the 6-h averaged sea level height.
114 The Baltic Sea bottom topography was downloaded from the Baltic Nest Institute portal (http://nest.su.se). The
115 initial bathymetric product of 1' × 1' resolution was recalculated to match the 2-mi resolution of the model grid.
116 On the solid boundaries, no-normal flow and free-slip boundary conditions for momentum were applied, and the
117 heat and salt fluxes were set to zero.

118   The mean monthly water temperature and salinity fields provided by the Copernicus Marine Service Information

119   portal (http://marine.copernicus.eu) were used for model initialisation. This product represents the output of the

120   three-dimensional baroclinic hydrodynamic ocean model HIROMB-BOOS-Model (HBM-V1), assimilating the

121   in situ vessel and satellite observations. The data cover the 1990–2009 period and contain the sea level, current

122   velocity, temperature, and salinity with a 5.6-km horizontal and 5-m vertical resolution.

123   The INMOM model was forced using ERA-Interim atmospheric reanalysis (Berrisford et al., 2011). The

124   reanalysis has a 0.75° spatial resolution and 6 h temporal resolution. The INMOM model used the following

125   forcing parameters: air temperature and humidity at an altitude of 2 m, atmospheric pressure at sea level, wind

126   speed of 10 m, precipitation, and short-wave and long-wave radiation.

127   The liquid boundary was drawn in the Kattegat Strait along 57.73°N (Fig 1) and defined using the Copernicus

128   mean monthly values of sea temperature and salinity, as well as the hourly sea level records on two tide gauge

129   stations, Frederikshavn (57.43°N, 10.57°E) and Goteborg Torshamnen (57.68°N, 11.79°E), located on the east

130   and west coast of the strait, respectively. In situ sea level measurements from these stations were interpolated to

131   the model grid nodes along the liquid boundary line.

132   Water level observations at 20 other gauging stations (Fig. 1) served to validate the model outputs. In situ data

133   were provided by the Copernicus Marine Service and the Northwest Hydrometeorological Service of Russia.

134   Table 1 presents the metadata of the stations used for validation. The *in situ* time series are sufficient for the

135   validation exercise and have only a few gaps. The percentage of missing data (found only for six stations) does

136   not exceed 6.1%. For the validation procedure, the *in situ* observations were averaged to match the 6 h output

137   frequency of the model.

138

139   **2.2 Model validation**

140

141   The sea level simulated by the basic INMOM configuration was verified against the in situ observations using a

142   set of standard statistical parameters: absolute (σ_{abs}) and relative (σ_{rel}) bias, root mean square error (σ_{er}), and

143   correlation coefficient (R). The standard deviation of the observed (σ_{tg}) and simulated (σ_m) sea surface height, as

144   well as their ratio (σ_p,), were evaluated, and the additional parameter of accuracy (P_m, %) were introduced. The

145   P_m parameter allows the assessment of the number of good simulations (comparing to total number of outputs)

146   considering their accuracy $< 0.674\sigma_{tg}$.

147

148

$$\sigma_{abs} = \frac{\sum_{i=1}^{N}\left|\zeta_m - \zeta_{tg}\right|}{N}, \tag{1}$$

149   where N is the time series length, ζ_m is the modelled sea level, and ζ_{tg} is the tide gauge observations.

150

$$\sigma_{rel} = \frac{\sigma_{abs} * 100\%}{(\zeta_{tg})_{\max} - (\zeta_{tg})_{\min}}, \tag{2}$$

151   where $(\zeta_{tg})_{\max}$ is the maximum and $(\zeta_{tg})_{\min}$ is the minimum value of the in situ observations.

152

$$\sigma_p = \frac{\sigma_{er} * 100\%}{\sigma_{tg}}, \tag{3}$$

$$R = \frac{\dfrac{1}{N-1}\sum_{i=1}^{N}(\zeta_{tg} - \overline{\zeta_{tg}})(\zeta_{m} - \overline{\zeta_{m}})}{\sigma_{tg}\sigma_{m}}$$

(4)
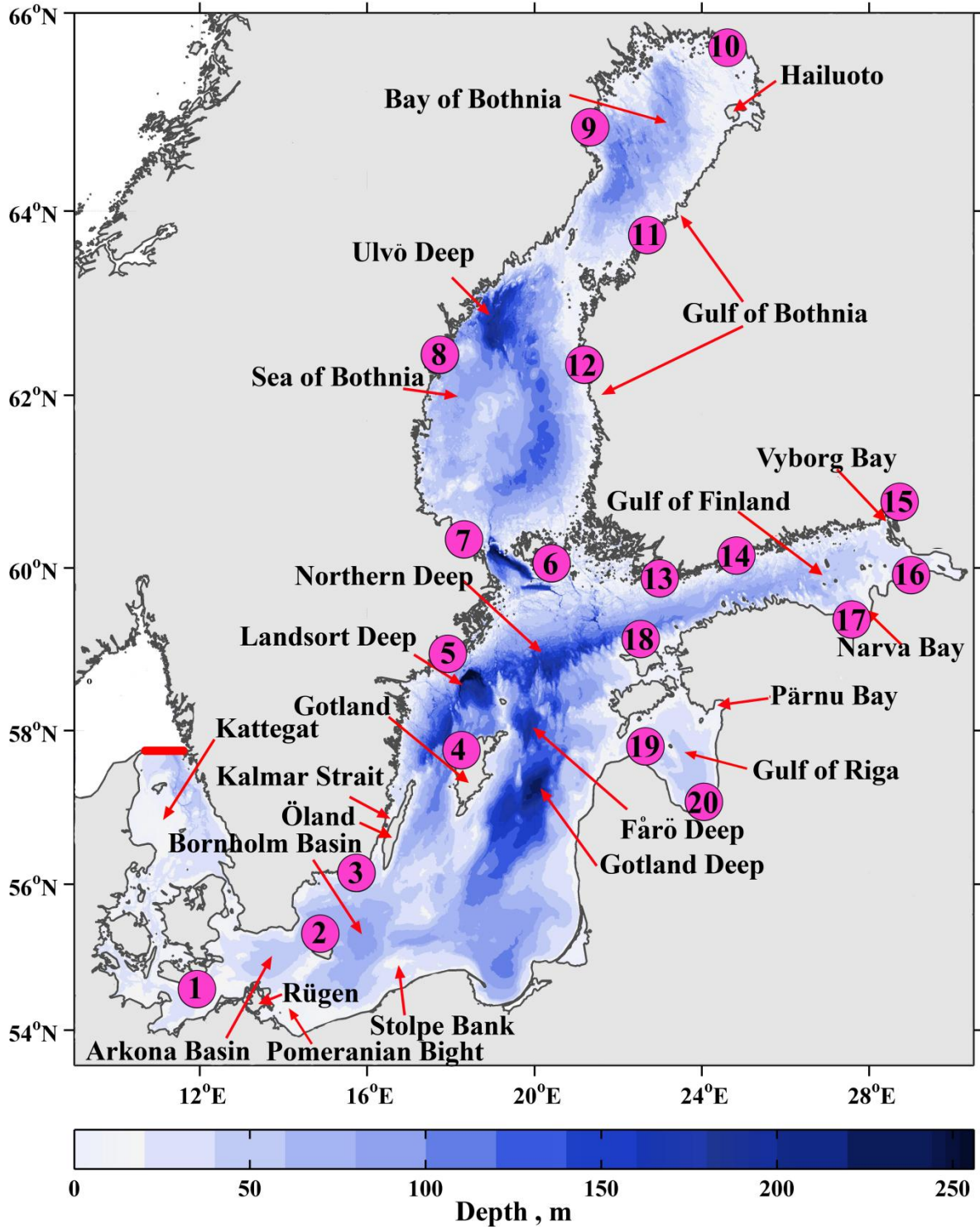
Figure. 1. Bathymetry and location of tide gauge stations used for model validation. The liquid boundary of the modelled area in the Kattegat Strait is indicated by bold red line. The map is created using Baltic Sea Bathymetry Database (BSBD) http://data.bshc.pro/

161 **Table 1. Tide gauge stations used in the study (state for study period 2009-2010).**

No	Station name	Coordinates		Measuring interval	Number of measurements	Missing values,%
		Lat. (°N)	Lon. (°E)			
1	Gedser	54.57	11.93	10 min	104093	1.3
2	Tejn	55.25	14.83	1 h	17338	1.0
3	Kungsholmsfort	56.11	15.59	1 h	17520	0.0
4	Visby	57.64	18.28	1 h	17520	0.0
5	LandsortNorra	58.77	17.86	1 h	17520	0.0
6	Degerby	60.30	20.38	1 h	17520	0.0
7	Forsmark	60.41	18.21	1 h	17520	0.0
8	Spikarna	62.36	17.53	1 h	17520	0.0
9	Furuogrund	64.92	21.23	1 h	17520	0.0
10	Kemi	65.67	24.52	1 h	17520	0.0
11	Pietarsaari	63.71	22.69	1 h	17520	0.0
12	Kaskinen	62.34	21.21	1 h	17520	0.0
13	Hanko	59.82	22.98	1 h	17520	0.0
14	Helsinki	60.15	24.96	1 h	17520	0.0
15	Vyborg	60.70	28.73	1 h	17520	0.0
16	Schepelevo	59.99	29.15	1 h	17520	0.0
17	Sillamae	59.42	27.74	1 h	16810	4.1
18	Lehtma	59.07	22.70	1 h	16465	6.1
19	Kolka	57.73	22.58	1 h	16520	5.7
20	Daugavgriva	57.05	24.02	1 h	17102	2.4

162

163 A comparison of the SSH model outputs and the observations from the gauging stations (Fig. 2) demonstrates

164 that the model reproduces the sea level variations in different parts of the Baltic Sea well. The correlation

165 between the simulated and observed time series was higher than 0.79. The absolute bias ranges within 6.7–9.2

166 cm, which represents 3.7–7.4% of the SSH magnitude at the gauging stations. Most of the model outputs (from

167 75% to 90%) have considerably good accuracy with respect to P_m parameter (Table2).

168

169 **2.3 Modelling free sea level oscillations in barotropic and baroclinic conditions**

170

171 To investigate the difference between free sea level oscillations in barotropic and baroclinic conditions, the

172 INMOM model was run in two different configurations.

173 In the barotropic configuration, the salt and heat fluxes were set to zero and the water density in the sea state

174 equation depended only on pressure. In the baroclinic configuration, the INMOM model took into account both

175 salt and heat fluxes, and the water density varied with pressure, temperature, and salinity. In both the barotropic

176 and baroclinic implementations, the Baltic Sea was considered a fully enclosed basin, with no water exchange

177 with the North Sea. The liquid border in the Kattegat Strait was assumed to be solid. This assumption aimed to

178 exclude the effect of external barotropic and baroclinic oscillations coming from the North Sea. River water
179 input and ice conditions were also neglected in both numerical experiments. Under natural conditions, the free
180 sea level oscillations attenuate rapidly due to the dissipative effects of vertical and horizontal viscosity, near-
181 bottom friction, non-linear effects, and Earth's rotation (Proshutinsky, 1993; Zakharchuk et al., 2004). According
182 to theoretical concepts and previous numerical experiments (Leppäranta and Myrberg, 2009; Proudman, 1953;
183 Wübber and Krauss, 1979; Zakharchuk et al., 2004), the relaxation of the Baltic large-scale free sea level
184 oscillations takes several days. In order to be able to characterize the free oscillations with better spectral
185 resolution and in larger spectral range, the sea level dumping factors have to be reduced. In both numerical
186 experiments, the dumping effect was reduced due to 1) setting the coefficients of vertical turbulent viscosity and
187 of bottom friction to zero and 2) setting the coefficient of horizontal turbulent viscosity to the minimum values.
188

189

190
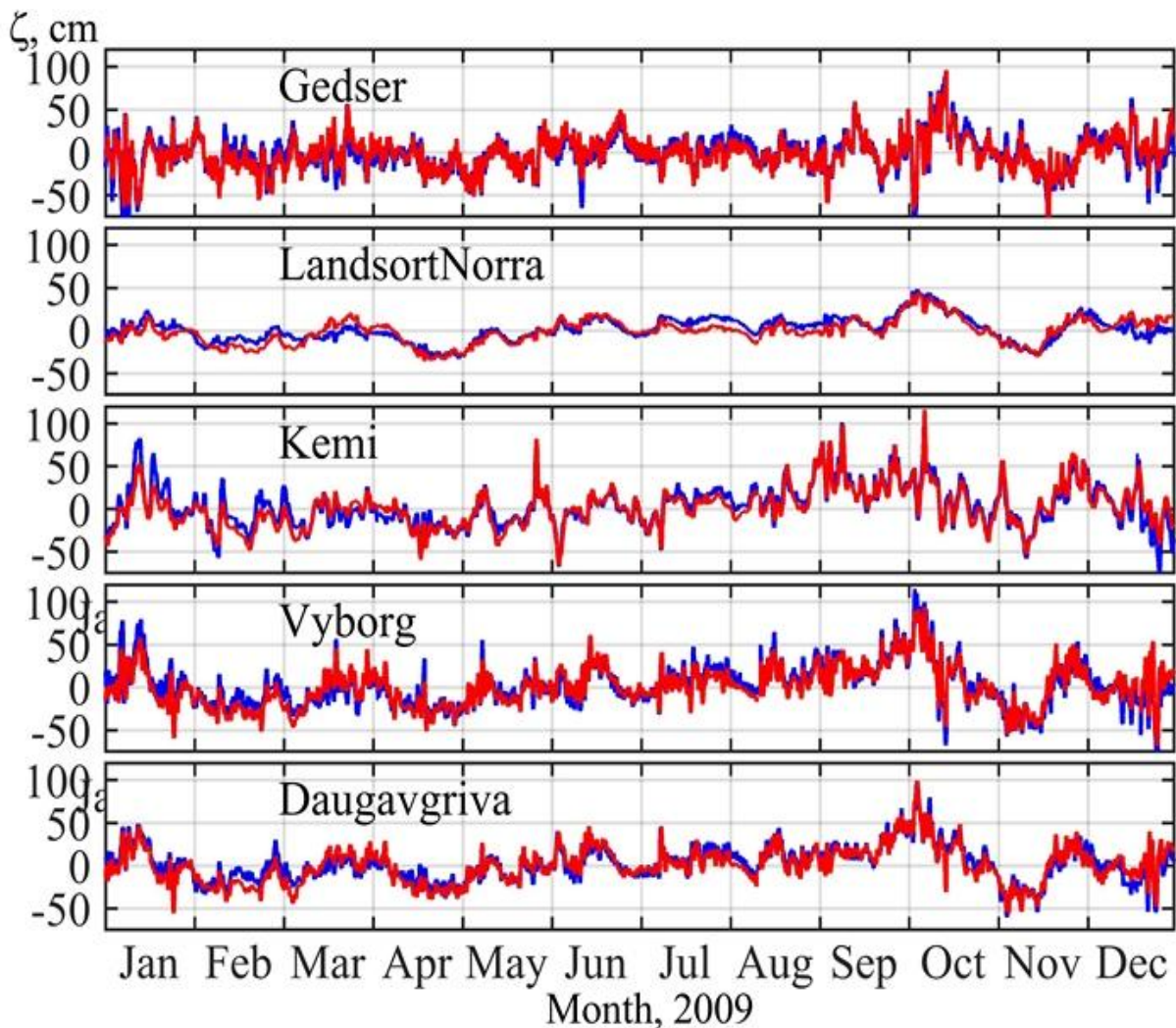
191 **Figure 2. Time series of in situ (blue) and modelled (red) sea level for 2009. The modelled dataset is derived from the**
192 **basic configuration of the INMOM model (see Section 2.1).**

193

194

195

196

197 **Table 2. Statistical scores evaluating the accuracy of the SSH model simulations.**

No	Station name	σ_{abs}, cm	σ_{rel},%	σ_{er}, cm	σ_m, cm	σ_{tg}, cm	σ_p%	P_m, %	R
1	Gedser	8.6	3.7	11.2	19.8	22.9	48.8	85.1	0.87
2	Tejn	7.4	3.9	9.5	14.2	17.0	56.0	80.2	0.83
3	Kungsholmsfort	7.6	4.7	9.7	14.4	16.2	59.7	77.9	0.81
4	Visby	7.0	6.5	9.1	12.3	14.7	61.8	77.6	0.79
5	LandsortNorra	7.2	7.4	9.2	12.8	14.7	62.5	75.4	0.79
6	Degerby	6.9	6.4	8.9	14.3	15.7	56.7	79.6	0.83
7	Forsmark	6.8	4.9	8.7	14.0	16.1	54.2	82.8	0.84
8	Spikarna	6.8	5.1	8.7	14.3	16.7	52.2	84.3	0.85
9	Furuogrund	7.0	4.4	9.2	18.3	20.6	44.4	88.3	0.90
10	Kemi	7.5	3.7	9.8	22.8	24.4	40.1	90.5	0.92
11	Pietarsaari	6.7	4.3	8.8	18.0	19.6	44.6	88.6	0.90
12	Kaskinen	6.8	4.4	8.8	15.9	17.6	49.9	85.9	0.87
13	Hanko	7.2	5.0	9.3	15.3	17.3	54.1	82.0	0.84
14	Helsinki	7.5	4.4	9.9	17.1	19.2	51.6	83.6	0.86
15	Vyborg	8.4	3.7	11.0	21.9	25.2	43.9	88.8	0.90
16	Schepelevo	8.7	3.7	11.4	21.3	25.0	45.8	87.6	0.89
17	Sillamae	8.0	4.1	10.3	19.5	21.7	47.8	85.5	0.88
18	Lehtma	9.2	6.1	12.1	16.5	20.2	60.2	76.3	0.80
19	Kolka	7.2	4.2	9.3	17.5	19.5	47.8	86.4	0.88
20	Daugavgriva	7.2	4.0	9.1	19.0	20.3	45.0	86.8	0.89

198

199

200 In both the barotropic and baroclinic numerical experiments, the model was perturbed for 10 days (1–10 January
201 2009) using ERA-Interim reanalysis. The meteorological forcing was then turned off and the simulations were
202 run for 2 years (2009–2010) considering only free dynamic oscillations.

203 At the end of the atmospheric forcing and the beginning of free sea level simulations, the southern part of the
204 Baltic Sea was under an atmospheric anticyclone centred over Central Europe, while the northern part of the sea
205 was affected by a low-pressure system that had developed over the Norwegian Sea. These meteorological
206 conditions resulted in prevailing western winds (Fig. 3a), and finally led to a 50–100 cm sea level increase in the
207 north and east and to a 30–50 cm sea level decrease in the southwest (Fig. 3b) parts of the Baltic Sea.

208 Fourier analyses of the simulated SSH time series were performed using the following decomposition.

209
$$f(t) = Z_0 + \sum_{k=0}^{N/2} (a_k \cos k\omega t + b_k \sin k\omega t) , \qquad (5)$$

210 where $\left(\omega = \dfrac{2\pi}{T} \right)$, f(t) is the sea level time series, N is the time series length, T is the period, t is the time, a_k is

211 the coefficient at frequency ω, Z_0 is the average of the sea level time series, and k is the coefficient number.

212   The phase (F_k) and amplitude (A_k) were calculated using Equation (5) for each model node, and their spatio-

213   temporal distribution was analysed.

214

215
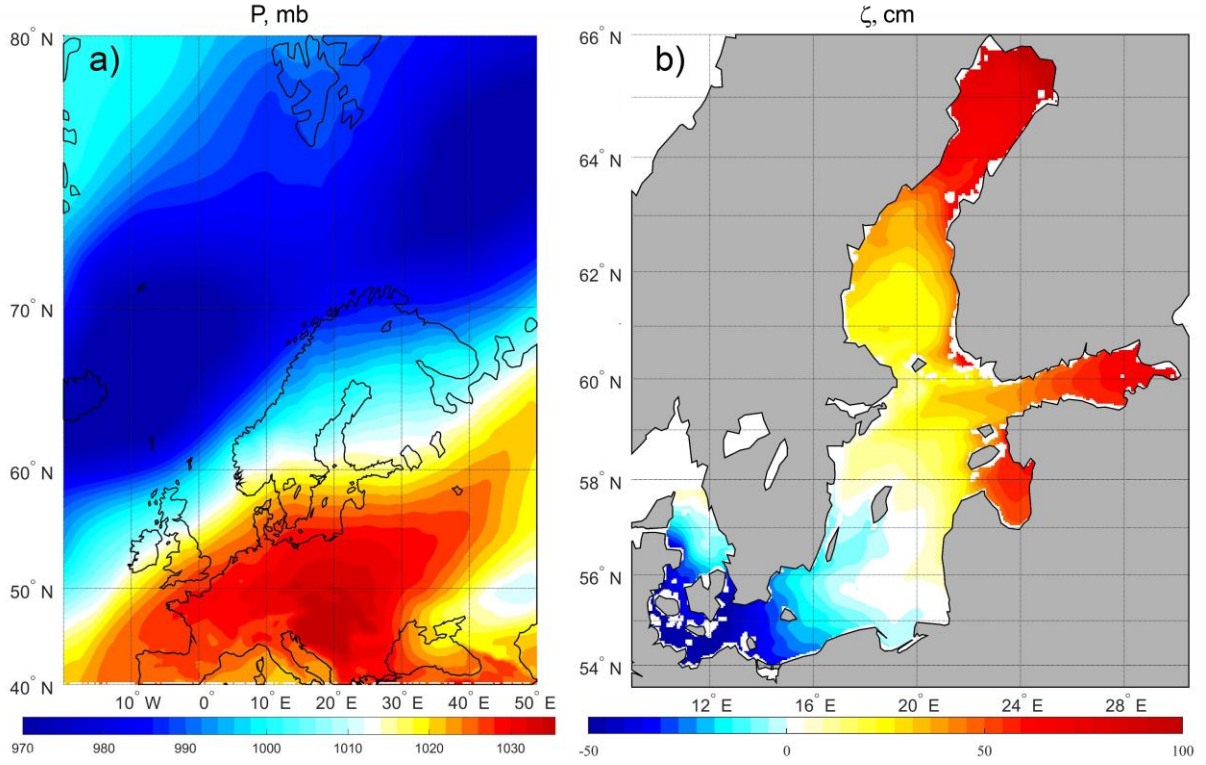
216   **Figure 3. ERA-Interim atmospheric pressure (a) and INMOM SSH (b) for the moment of cessation of atmospheric**

217   **forcing (10 January 2009, 18 h).**

218

219    $$A_k = \sqrt{a_k^2 + b_k^2} \; , \; F_k = \arctan\left(b_k / a_k\right).$$ (6)

220   The wave phase velocity (C) was estimated using the phase difference between adjacent nodes:

221    $$C_x = \frac{\Delta x \cdot 360}{T \Delta F_x} \, , \; C_y = \frac{\Delta y \cdot 360}{T \Delta F_y} \, ,$$ (7)

222    $$C = \sqrt{C_x^2 + C_y^2} \, ,$$ (8)

223

224   where C_x and C_y are zonal and meridional components of the wave phase velocity, ΔF_x and ΔF_y are the zonal and

225   meridional phase difference in degrees, respectively, and T is the period.

226   The estimation of the phase speed was performed only for regions where $A_k > 0.67\sigma$ (Guide, 1994).

227    $$\sigma = \sqrt{\frac{A^2}{2}} \, ,$$ (9)

228   where A is the field average sea level amplitude at each frequency ω.

229

230

231   **3 Comparison of simulations of free barotropic and baroclinic sea level oscillations**

232   **3.1 Free barotropic oscillations**

233

234 In general, simulated free barotropic sea level oscillations in the Baltic Sea range within 3–15 cm depending on

235 the region (Fig. 4). The maximum amplitudes are noted in the eastern Gulf of Finland. The minimum values

236 occur in the central part of the Baltic proper.

237 The standard deviation (σ_m) of the sea level estimated for each grid node can be used for the characterisation of

238 the oscillation intensity. The spatial distribution of the σ_m values demonstrates that the highest barotropic

239 oscillations (σ_m of 2.5–5 cm) can be found in the Neva Bay of the Gulf of Finland, in the northern Bay of

240 Bothnia near Hailuoto Island, as well as in the Kalmar Strait near the southeast Sweden coast (Fig. 5). Barotropic

241 oscillations of medium intensity (σ_m of 1–2 cm) are observed in the Pärnu Bay of the Gulf of Riga, northeast of

242 the Baltic proper, near Rügen Island, as well as in the Danish straits and Kattegat Strait. Oscillations of medium

243 intensity occur in area of local uplifts in the Baltic proper, in area of the Ulvö Deep, the Landsort Deep, the

244 Northern Deep and the Gotland Deep. These local spots have not been observed in previous experiments to be

245 effectuated using a shallow-water model (Jönsson et al., 2008). In the shallow-water equations, the water

246 movement is independent of the vertical coordinate. Sea level fluctuations are generated only due to full flux

247 divergence and surface slope related to geostrophic balance. In regions with sharp bathymetry (uplifts, sills,

248 deeps), the generation of relatively high perturbations of the vertical component of the speed of barotropic flux is

249 probable. These perturbations may not be negligible and, presumably, affect sea level fluctuations.

250 The Fourier analysis of the simulated time series of free barotropic sea level oscillations (Fig. 6) indicates that

251 amplitude peaks frequently occur at periods of 13, 15–16, 19, 23, 27, 29, 41, and 44 h. Near the Gulf of Finland

252 and in the southeast Baltic proper, the period of the highest amplitude peak is 13 h. In the inner Gulf of Finland,

253 oscillations of 27-h periods became prevalent. The barotropic free oscillations of this period dominate in the

254 northern Gulf of Bothnia and south-western Baltic proper. Other significant oscillations of 15, 23, 29, and 41 h

255 are also observed in the Gulf of Finland. However, their amplitude is 2–4 times lower than that of 27 h period

256 oscillations.

257 In the south-eastern and eastern Baltic proper, free barotropic oscillations of 13 and 41 h periods have the highest

258 amplitudes. In the centre of the Bothnia Sea, the dominant oscillation has a 19.5-h period. In the Gulf of Riga,

259 the highest amplitude was observed as 23 h barotropic oscillations. This result differs from the 17-h period found

260 in the study by Jönsson (Jönsson et al., 2008) based on the shallow-water model.

261 Nevertheless, a portion of our results is consistent with those determined by a numerical experiment conducted

262 by Wübber and Krauss (Wübber and Krauss, 1979), where, similar to our study, the effect of the Earth's rotation

263 was taken into account. These authors identified eigenoscillations with periods of 31.0, 26.4, 22.4, 19.8, 17.1,

264 and 13.0 hours. In our experiment, the corresponding periods were 31, 27, 23, 20, 16, and 13 hours. Moreover,

265 owing to the more sophisticated 3-D model, higher spatial resolution of the grid, and longer period of

266 simulations (716 days), we were able to improve both the spectral resolution of the simulated time series and

267 their spectral range. We identified additional free barotropic oscillations of periods of 44, 41, 37, 29, 21, 16, and

268 15 h that have not been noted previously.

269 An analysis of the spatial distribution of the amplitude and phase of free barotropic oscillations with periods of

270 13, 27, and 41 h (Fig. 7) demonstrates that due to the Earth's rotation and the enclosed configuration of the sea,

271 these oscillations transform into progressive-standing waves (PSW). Similar to the amphidromic systems of tidal

272 waves (Nekrasov, 1975; Pugh, 1987; Voynov, 2003), there are no sea level oscillations in the PSW nodes, while

273 in the PSW, the oscillations are maximised. The progressive-standing waves of 13 h periods have 10 nodes (Fig.

274 7a). Their maximum amplitudes are observed in their antinodes located in the Danish straits and eastern Gulf of
275 Finland.

276
277
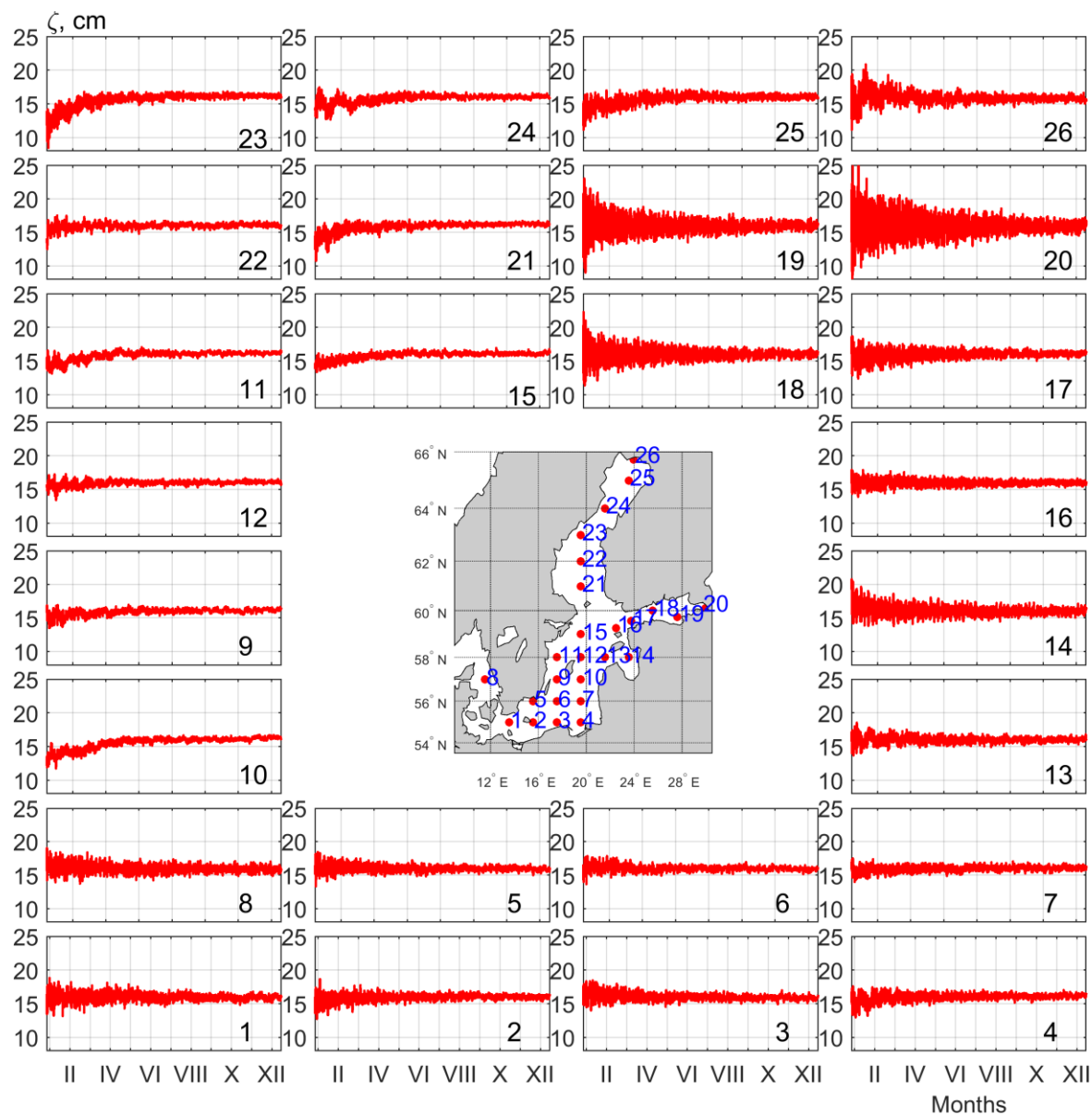
278
279 **Figure 4. Time series of free barotropic sea level oscillations at selected points simulated by INMOM model. Location**
280 **of points is shown on the map.**
281
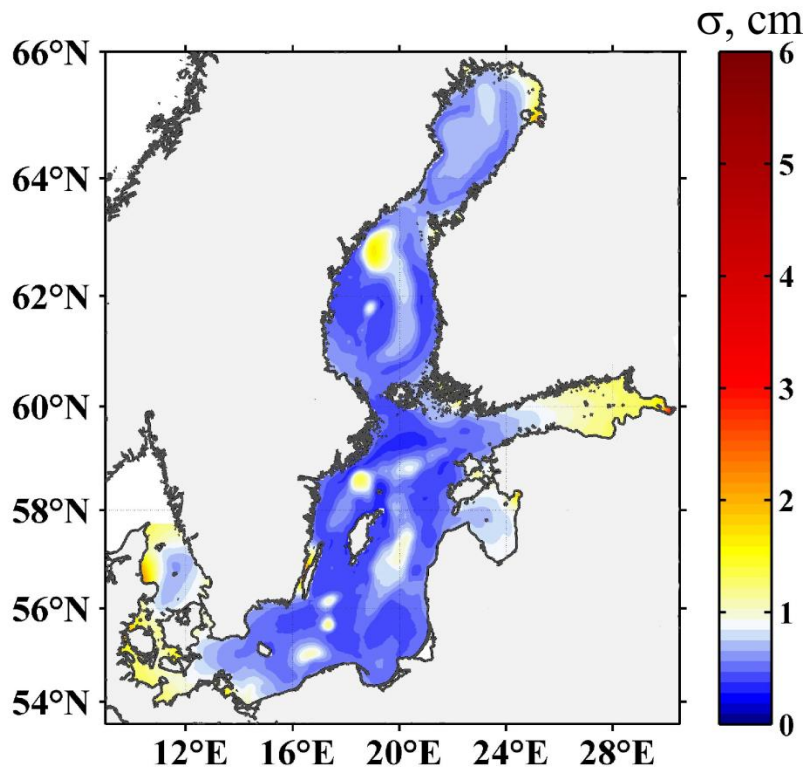
Figure 5. Sea level standard deviation (σ) for free barotropic oscillations simulated by INMOM model.

The location of our 13 h amphidromic systems in the Gulfs of Bothnia, Finland, and Riga agrees well with the results found by Wübber and Krauss (Wübber and Krauss, 1979) for the 13.04 h eigenoscillations. However, for the Baltic proper, our systems (near the Fårö and Bornholm Deeps) are shifted by 200 km toward the northeast. Another significant difference is the direction of isophase rotation, which in our experiment occurs clockwise, while Wübber and Krauss suggested an anticlockwise rotation.

Free barotropic oscillations of 27 h periods have two predominant amphidromic systems: one is in the Bothnia Sea and the second is to the northeast of Gotland Island (Fig. 7b). Their location is consistent with the location of the corresponding eigenoscillation of the 26.4 h period of Wübber and Krauss. Our simulations allowed the detection of several more degenerate amphidromic systems of 27 h periods, which have not been reported by previous studies. Degenerate amphidromic systems were found in the northern Bothnia Sea, the Aland Sea, the central and south-eastern parts of the Gulf of Bothnia, at the exit of the Gulf of Finland, and in the Great Belt and Sound Straits. The PSW antinodes with 27 h periods have variable amplitudes, with the highest amplitude located in the eastern Gulf of Finland. Antinodes with lower amplitudes are situated in the northern Gulf of Bothnia, to the southeast of the Aland Islands, in Pärnu Bay of the Gulf of Riga, and in the south-western Baltic proper. In contrast to the 13 h amphidromic systems, the isophase rotation in the main 27 h systems occurs anticlockwise.
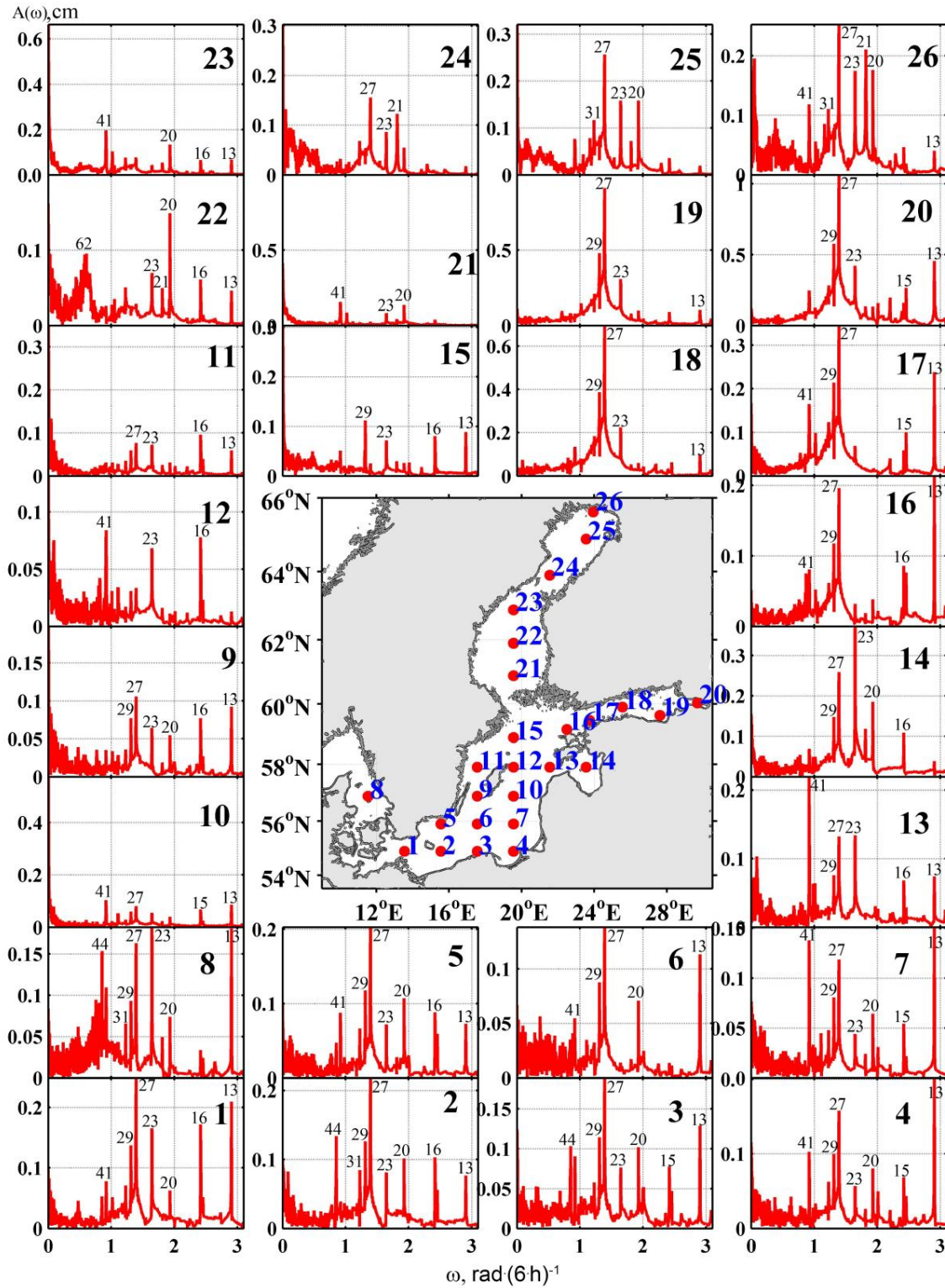
Figure 6. Amplitude spectra A(ω) of free barotropic oscillations in different parts of the Baltic Sea. Numbers above the peaks show oscillation periods in hours. Locations of points are shown on the map.

Free barotropic oscillations of 41 h periods are characterised by larger amounts of amphidromic systems (Fig. 7c). Their primary systems are detected in the northern and central Gulf of Bothnia, Bothnia Sea, eastern Gulf of Finland, Kattegat Strait, and Danish straits. Numerous degenerate amphidromic systems can be seen in the north, east, and central parts of the Baltic proper, along its southern coast, the easternmost part of the Gulf of Finland,

310 and in the Danish Straits. The amplitude of the free 41 h oscillations is 2 times lower than that of the 27 h period

311 waves. The most noticeable PSW antinodes are localised within the narrow areas of the coastal zones in the

312 northern and eastern parts of the Gulf of Bothnia, in the Neva Bay of the Gulf of Finland, along the western,

313 eastern, and southwestern coasts of the Baltic proper, as well as in the Danish and Kattegat Straits. The isophases

314 of 41 h oscillations rotate in a clockwise direction, similar to the 13 h period waves.

315
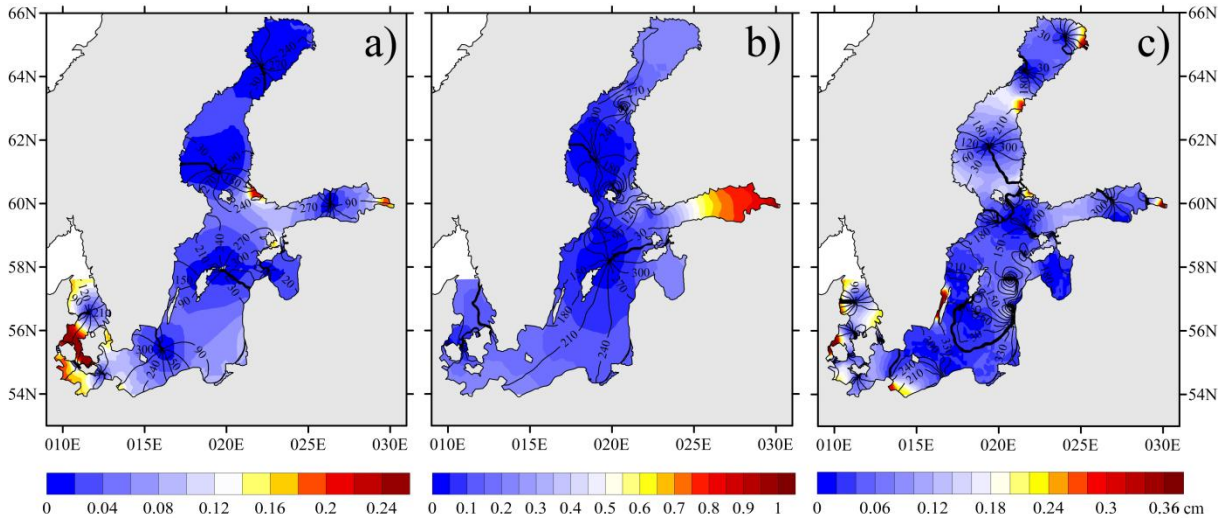
317 **Figure 7. Maps of amplitudes (in cm) and phases in degree (isolines) of free barotropic sea level oscillations with 13 h**

318 **(a), 27 h (b), and 41 h (c) periods.**

319

320 An estimation of the phase speed (C) of the PSW using Equations (7) and (8) demonstrates that C reduces with

321 an increase in the wave period (Fig. 8). For the 13 h PSW, the phase speed can reach 40 m s^{-1}, for the 27 h PSW,

322 only 19 m s^{-1}, and for the 41 h PSW, it can reach 13 m s^{-1}. In areas where ΔF_x and ΔF_y equal to zero (white areas

323 on fig 8), the standing wave component prevails.

324 The average depth of the Baltic Sea and its main gulfs varies from 15 to 77 m, while the maximum values reach

325 14–458 m (Leppäranta and Myrberg, 2009). Under these conditions, the theoretical phase speed of the barotropic

326 gravity wave in the Baltic Sea, calculated using expression $C_g = \sqrt{gH}$ (where H is the depth and g is the

327 acceleration due to gravity), ranges between 12 and 67 m s^{-1}. Most of our C estimates for the 13 h waves are

328 within this theoretical range (Fig. 8b). For only 70% of the detected 27 h waves, the phase speed agrees with the

329 theoretical values (Fig. 8d), while among the PSWs of 41 h period, waves that are lower than the theoretical

330 phase speed dominate (Fig. 8f).

331

332 **3.2 Free sea level oscillations in baroclinic conditions**

333

334 In stratified basins along with high-frequency (daily and hourly scales) oscillations, the low-frequency free

335 oscillations of the seasonal scale are also generated after the meteorological forcing ceases. These phenomena

336 have periods from several months to one year and reach 30–35 cm in range (Fig. 9).
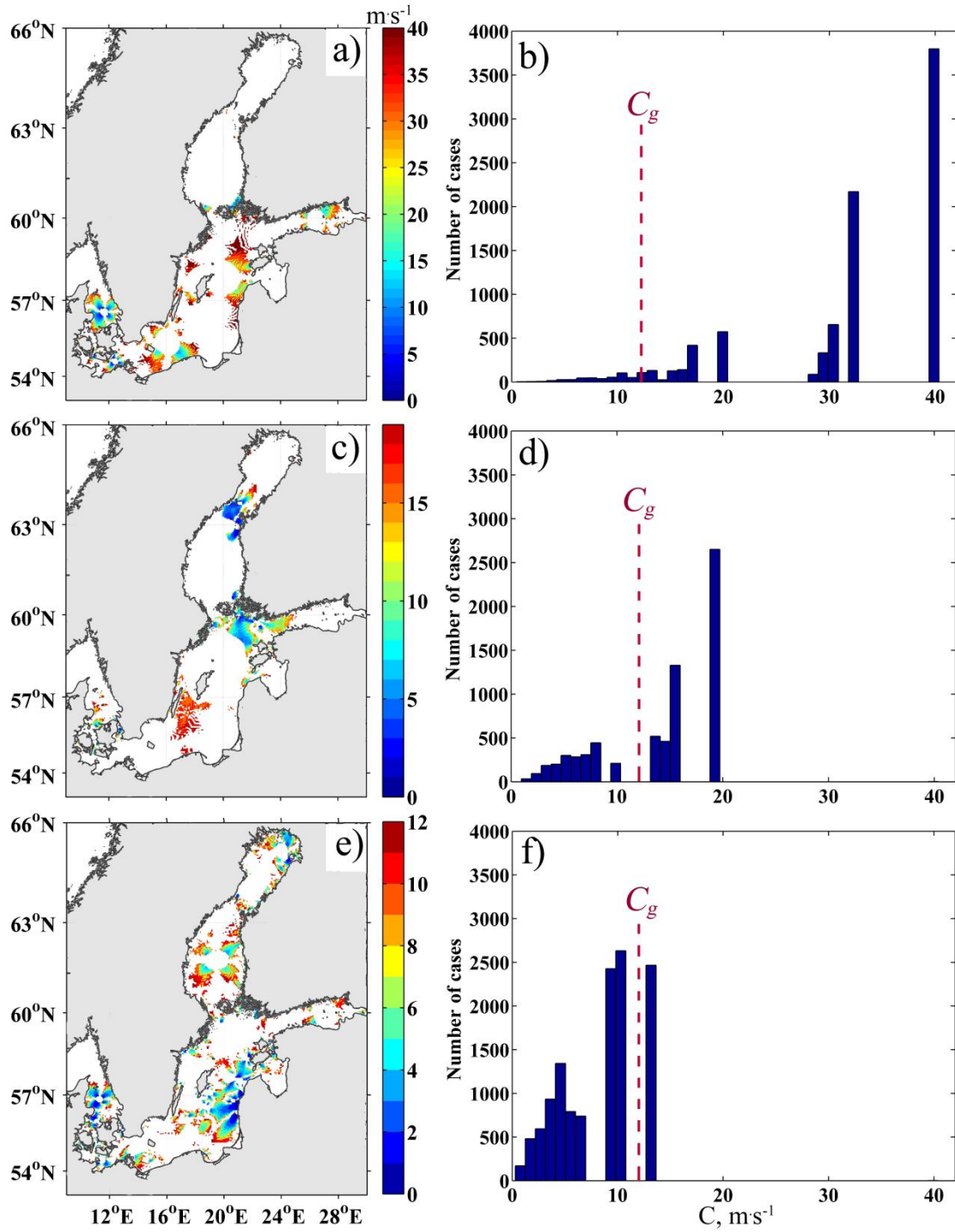
Figure 8. Maps and histograms of phase speed of barotropic progressive-standing waves of 13 h period (a,b), 27 h period (c,d) and 41 h period (e,f). In the regions colored in white the estimated phase speed equals to zero. Dash line on the histogram plots indicates minimum theoretical value of phase speed of barotropic gravity wave (Cg).

342
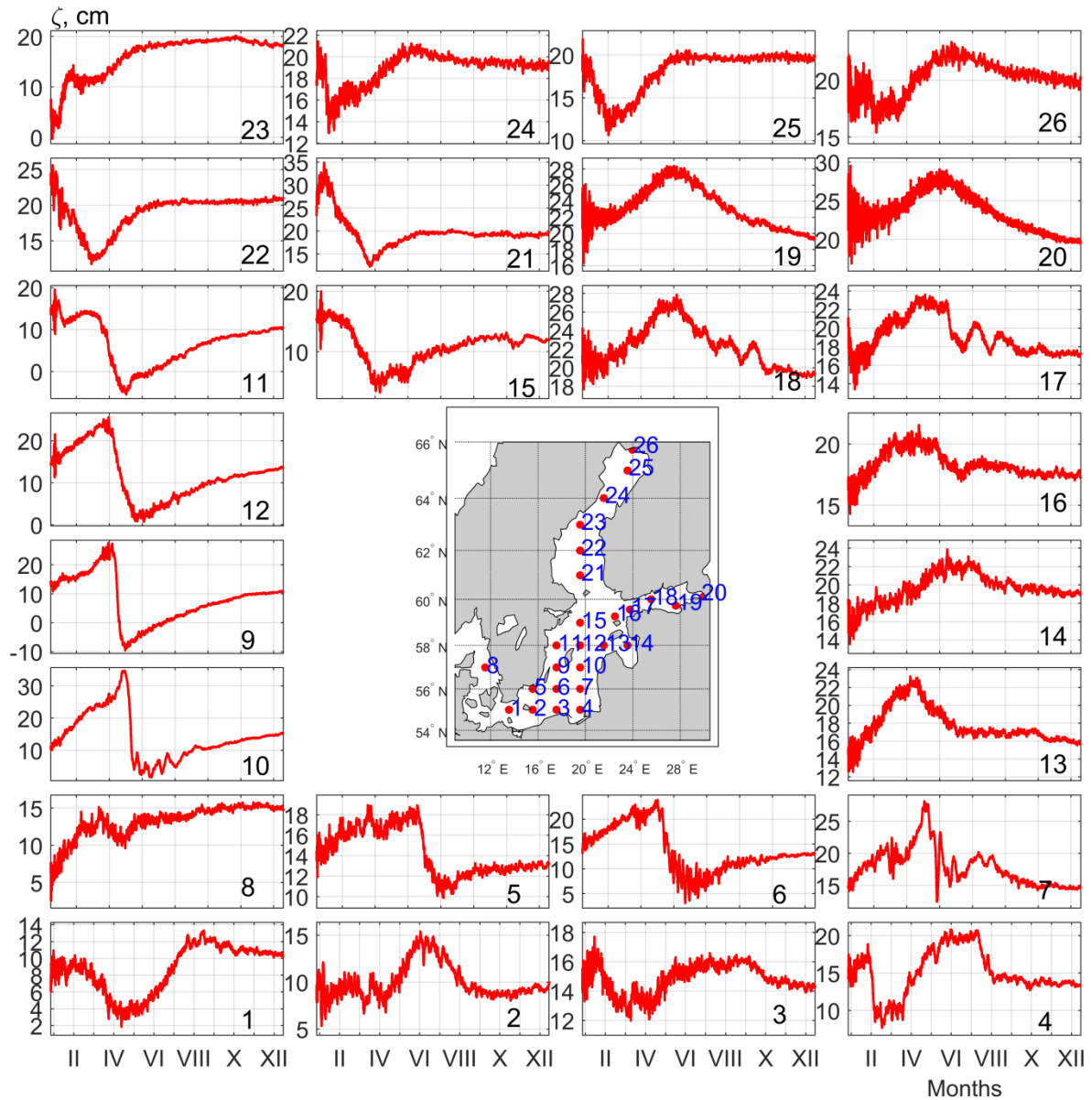
Figure 9. Time series of free sea level oscillations in baroclinic conditions at selected points simulated by INMOM model. Location of points is shown on the map.

343
344

345

346 The spatial distribution of the standard deviation of the amplitudes of the free oscillations in the baroclinic sea
347 (Fig. 10) demonstrates that the location of the zones with a high SSH variability is similar to that found in the
348 barotropic experiment. These are the deep-water basins of the Baltic proper: Landsort Deep, Farö Deep,
349 Northern Deep, and Gotland Deep, as well as the Ulvö Deep in the Sea of Bothnia. The σ_m values in the
350 baroclinic experiment were 4–6 times higher than in the barotropic study. We also identified several zones of
351 moderate SSH variability, which were not detected in the barotropic simulations. They are situated in the south-
352 eastern Sea of Bothnia, central Gulf of Finland (off the Narva Bay), the straits between the Öland and Gotland
353 Islands, and central Arkona Basin.

354
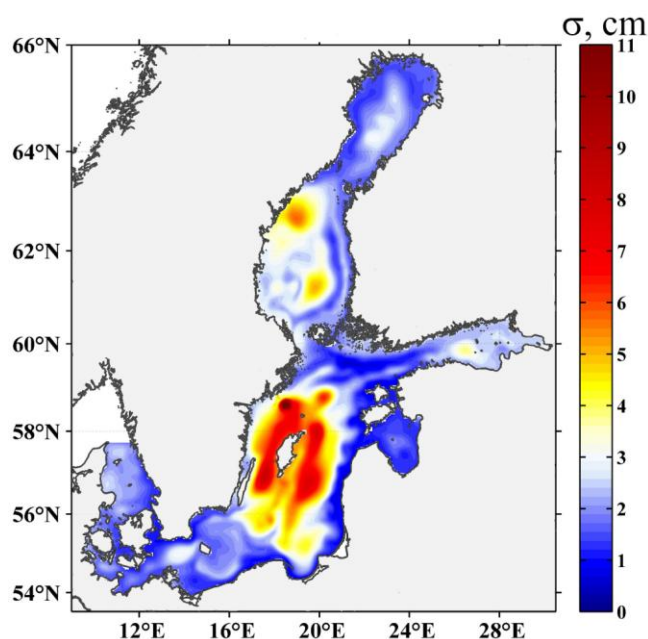
Figure 10. Sea level standard deviation (σ) for free oscillations in the baroclinic sea, simulated using INMOM model.

The Fourier analysis demonstrates that in baroclinic conditions, the maximum energy concentrates mostly at low frequencies. However, the differentiation of distinct peaks in low-frequency bands is problematic (Fig. 11).

In higher frequencies, the energetic maximums correspond to those found in the barotropic experiments (e.g. to peaks with periods of 13, 19, 23, 27, and 41 h). The difference with the barotropic experiment consists of a decrease in the peak amplitude along with an increase in width. This difference could be explained by the following two factors: 1) the stratification for barotropic free sea level oscillations can work as a dissipative factor; 2) when a barotropic current interacts with sharp bathymetry, the vertical component of the current significantly increases. This component affects the pycnocline and generates baroclinic oscillations with frequencies close to the barotropic oscillations. The resulting oscillations became amplitude-modulated and their spectral peaks broaden.

For comparison with the barotropic experiment, the spatial distribution of the amplitudes and phases of the 13 h, 27 h, and 41 h oscillations in baroclinic conditions is shown in Fig. 12. In a stratified sea, the amplitude of the 13 h and 27 h oscillations is two times lower. For lower-frequency waves (41 h), the difference with barotropic conditions is negligible. The highest amplitudes for the 13 h periods are observed in the eastern Gulf of Finland and in Vyborg Bay (Fig. 12a). In the stratified environment, the 13 h amphidromic systems disappear in the Gulf of Bothnia and Gulf of Finland, as well as in the central Baltic proper. The systems remain detectable only in the southern Baltic Sea and in the Kattegat Strait. Free oscillations of 27 h periods in the baroclinic conditions reached the maximum in the eastern Gulf of Finland (Fig. 12 b). The 27 h amphidromic system is observed only in the central part of the Baltic.

The spatial structure of the 41 h free oscillations in the baroclinic conditions was similar to that found in the barotropic experiment. The oscillations of higher intensity are observed within small coastal areas in the north and east of the Gulf of Bothnia, in the Neva Bay of the Gulf of Finland, along the west and southwest coasts of the Baltic proper, as well as in the Danish and Kattegat Straits (Fig. 12 c). The location of the 41 h amphidromic systems in the baroclinic conditions in many areas (north of the Gulf of Bothnia, the Bothnia Sea, east of the Gulf of Finland, the Kattegat Strait, and the Danish straits) is similar to that found in the barotropic experiment.

383   However, in stratified conditions, the degenerate amphidromic systems change. One system in the east of the
384   Baltic proper disappears, while a new appears in the south-eastern section of the sea (Fig. 12 c).

385

386
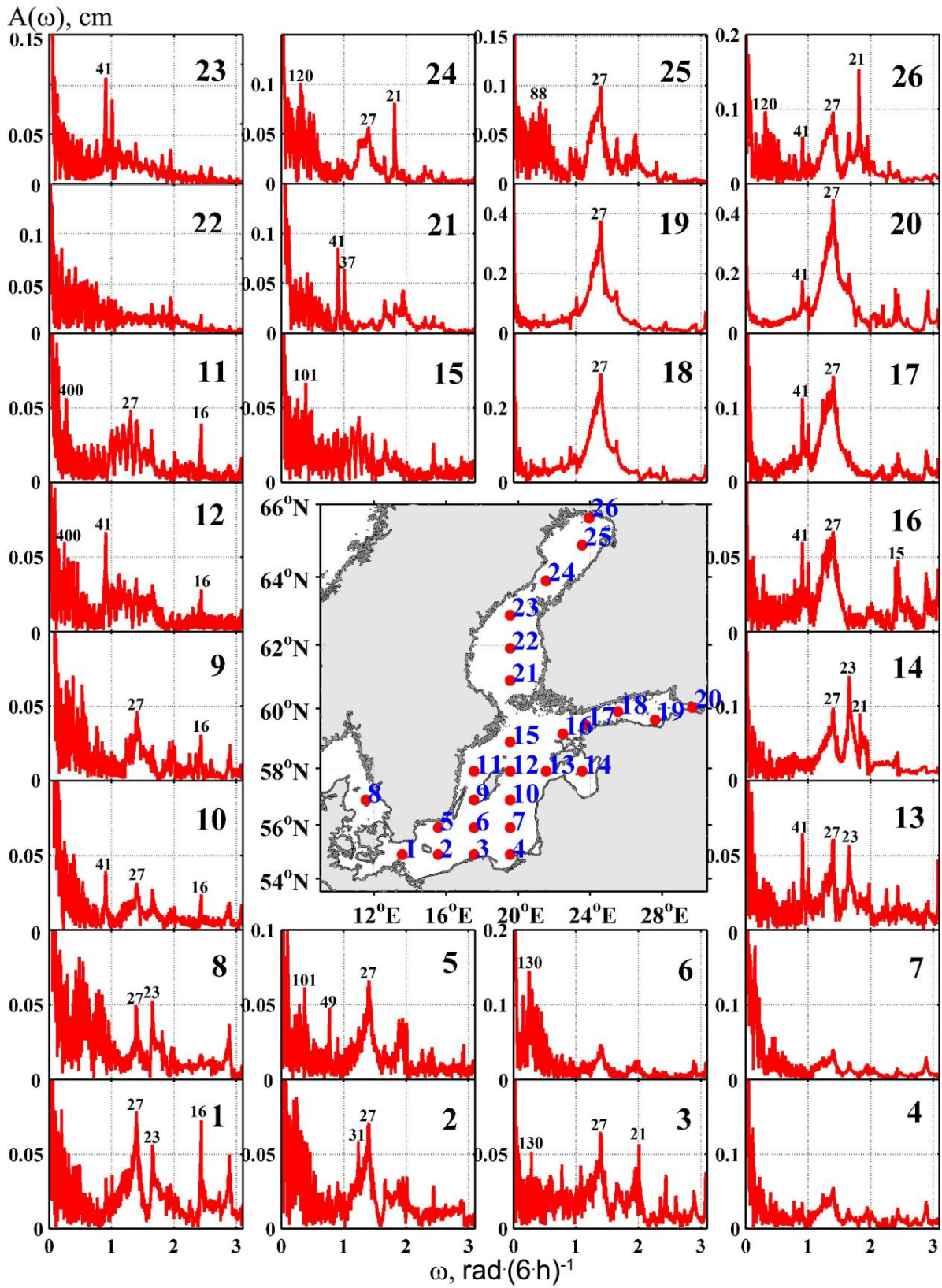
387   **Figure 11. Amplitude spectra A(ω) of free oscillations in baroclinic conditions in different parts of the Baltic Sea.**
388   **Numbers above the peaks show oscillation periods in hours. Locations of points are shown on the map.**
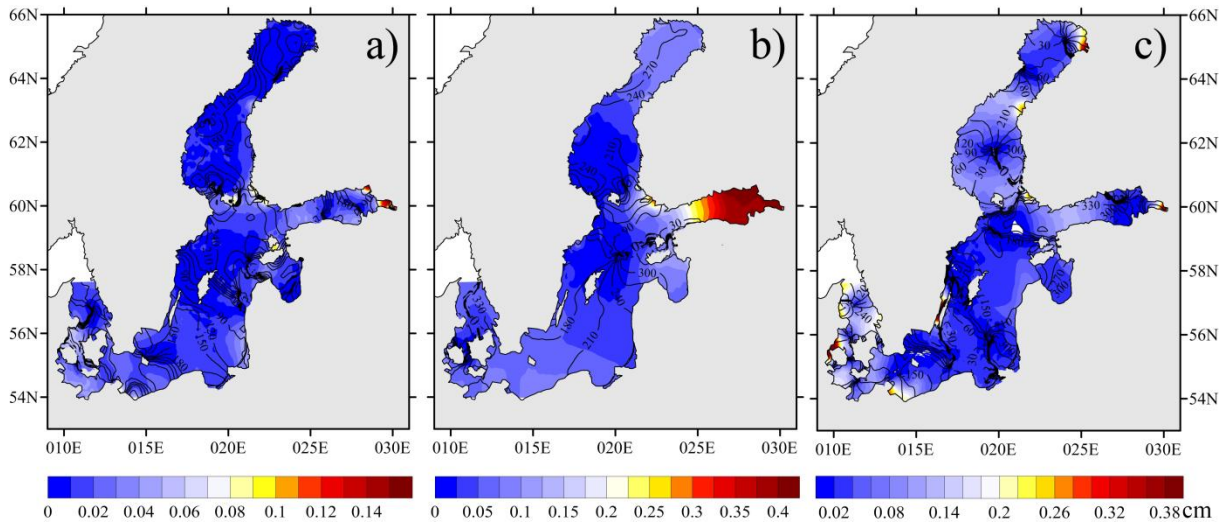
Figure 12. Maps of amplitudes (in cm) and phases in degrees (isolines) of free sea level oscillations with 13 h (a), 27 h (b) and 41 h (c) periods in the baroclinic sea.

The phase speed of the PSW movement in the baroclinic conditions varies within 2–37 m s^{-1} for the 13 h waves, 1–20 m s^{-1} for the 27 h waves, and within 1–13 m s^{-1} for the 41 h waves (Fig. 13).

To interpret the detected free-sea level oscillations in baroclinic conditions, we compared the estimated phase speed of the modelled oscillations with the theoretical phase speed values of the baroclinic gravity waves. The theoretical dispersion relation of an internal gravity wave (C_i) calculated for the 1.5-layer model (Carmack and Kulikov, 1998) can be estimated using expression $C_i = \sqrt{g'h'}$, where g is replaced by $g' = \dfrac{\Delta\rho}{\rho}g$ (ρ is mean sea water density, $\Delta\rho$ is difference in the densities between two layers, and h' is upper sea layer depth).

Using the Copernicus data of the vertical distribution of sea water density for 2009–2010, we estimated the phase speed of the internal gravity waves (C_i) for the entire Baltic Sea. For variables ranging from 2 to 60 m (h'), $3.0–40 \times 10^{-4}$ ($\Delta\rho/\rho$), and $2.9–39 \times 10^{-3}$ m s^{-1} (g'), the phase speed of the internal gravity waves must vary within 0.08–1.53 m s^{-1}.

Our estimations of the phase speed (C) of free oscillations in the baroclinic medium using Equations (7) and (8) for waves with 13, 27, and 41 h periods do not coincide with the range of theoretical phase speeds of the internal gravity waves (C_i) in the Baltic Sea. Most of our C estimations for the 13 h, 27 h, and a significant portion of the 41 h baroclinic oscillations are within the range of theoretical values calculated for the barotropic conditions (see Section 3.1).

The spatial structure of free baroclinic oscillations of 89 days and 358 days (Fig. 14) agrees well with the spatial distribution of the sea level standard deviation for the free oscillations in the baroclinic sea (Fig. 10). This means that the overall spatial structure of the free oscillations in baroclinic seas is determined mostly by oscillations at seasonal scales. The highest amplitudes of the long-period waves are observed in the deep regions of the Baltic proper and Bothnia Sea. Moreover, a significant spatial variability in their phases can be noted.

Nodal lines of these waves traverse the sea between the coasts in different parts. In areas of isophase condensation, where the amplitudes of sea level oscillations are near 0, the phase can reverse to the opposite. In

417   other areas, the phase of 358 day oscillations can change gradually. This confirms the likely presence of a low-

418   frequency progressive component of wave movement, which is oriented mostly in the southern direction (Fig.

419   14a).

420

421
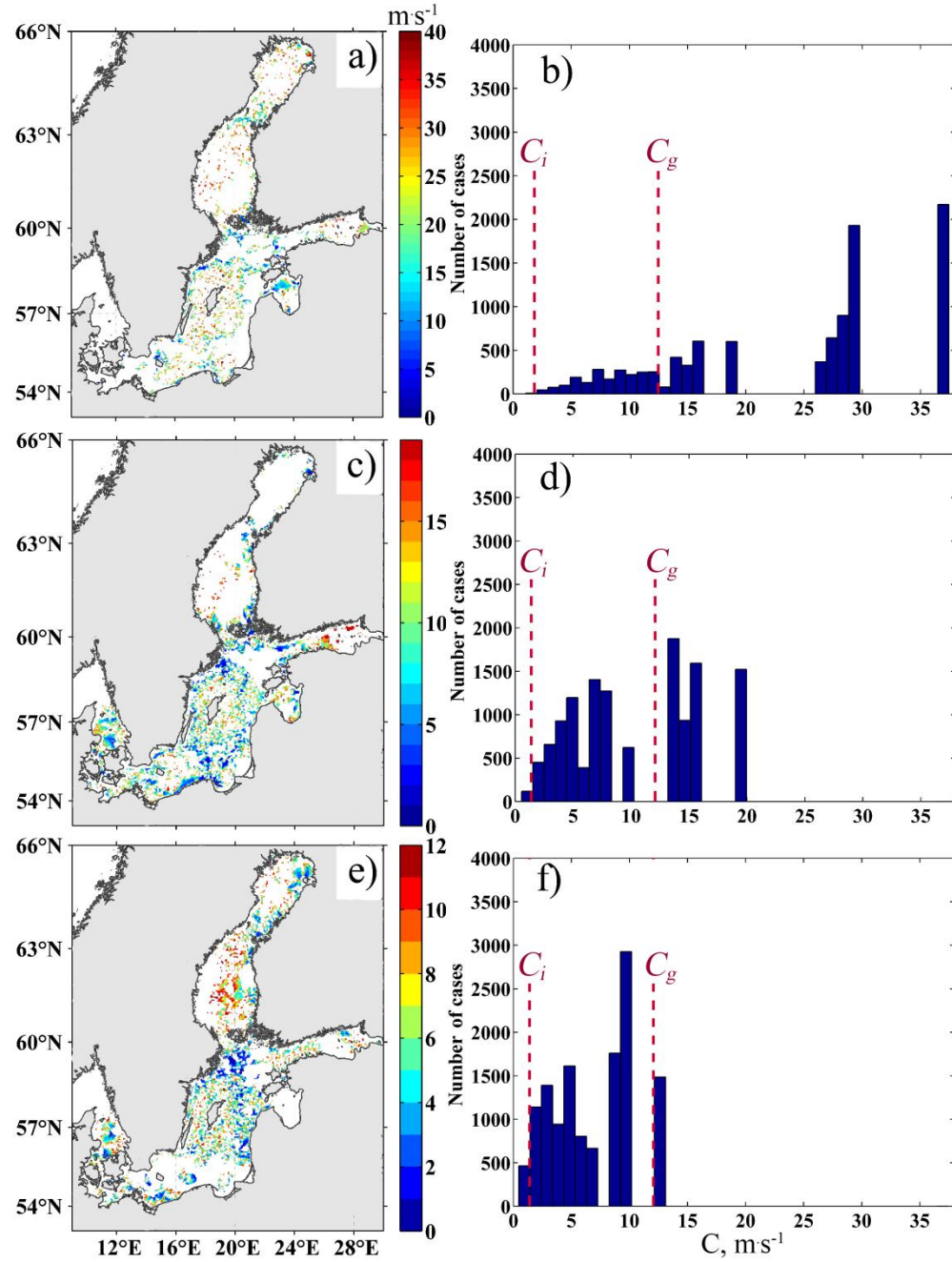
422   **Figure 13. Maps and histograms of phase speed of progressive-standing waves of 13 h period (a,b), 27 h period (c,d)**

423   **and 41 h period (e,f) in the baroclinic sea. In the regions colored in white, the estimated phase speed equals to zero.**

424   **Dash line on the histogram plots indicates maximal theoretical value of phase speed of baroclinic gravity waves (C_i)**

425   **and minimal theoretical value of phase speed of barotropic (C_g) gravity waves.**
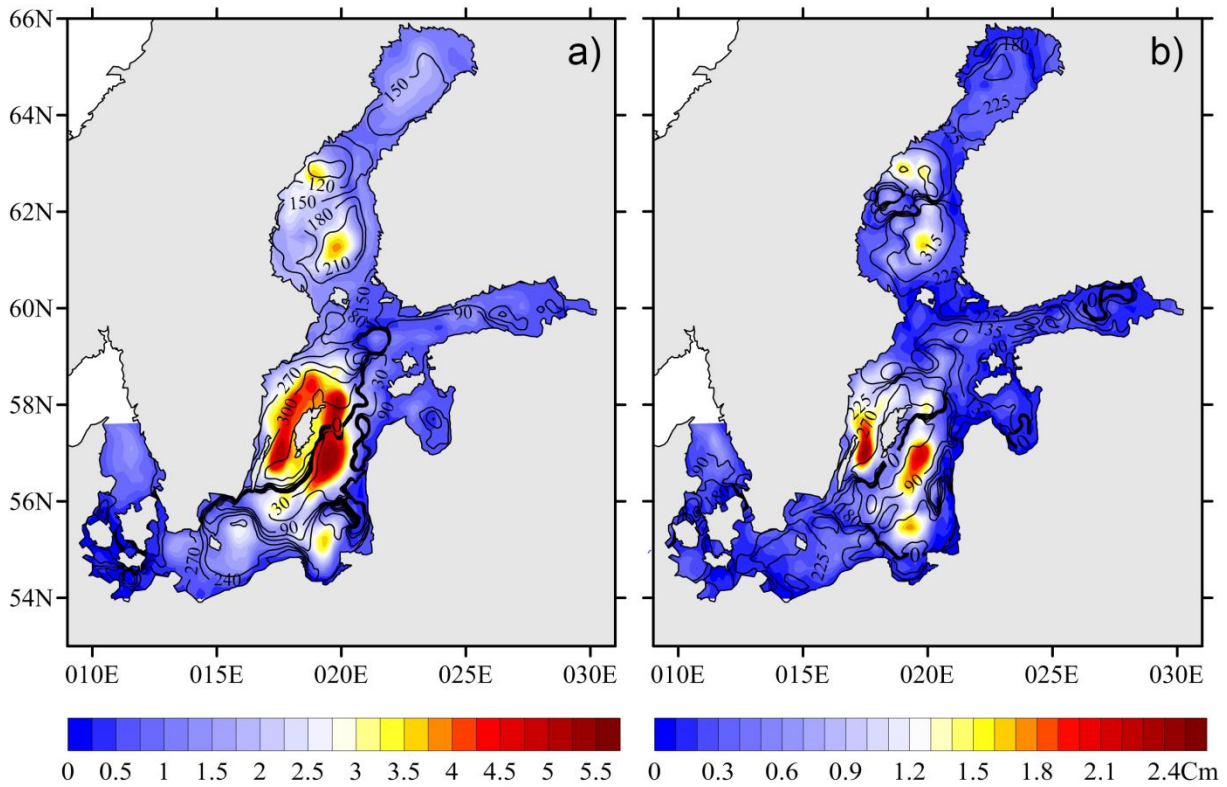
Figure 14. Amplitudes in cm (colour) and phases in degrees (co-tidal lines) of the free sea level oscillations in the baroclinic sea on periods 358 (a) and 89 (b) days.

Free baroclinic oscillations of 89 days have degenerate amphidromic systems in the southwest, south, and northwest Baltic proper. These systems rotate in a anticlockwise direction (Fig. 14 b). The phase velocity of the seasonal PSWs vary within 0.01–0.07 m s^{-1} and within 0.01–0.24 m s^{-1}, respectively for 358-day and 89-day oscillations. For 358-day waves, our estimations of the phase speed are significantly lower than that of the theoretical internal gravity waves (C_i). For 89-day waves, the part of our estimations belongs to the range of phase speed of internal gravity waves.

Regarding the theoretical phase speed of the internal gravity waves (C_i), these values are significantly lower for longer waves and belong to the theoretical range for waves of the shorter period(Fig.15).

4 Discussion

Our numerical experiments based on a three-dimensional hydrodynamic model demonstrated that after the cessation of meteorological forces, the return of the Baltic Sea water mass to equilibrium in barotropic and baroclinic conditions is different.

In barotropic conditions, the most intense free oscillations occur on a time scale of 13, 15–16, 19, 23, 27, 29, 41, and 44 h. The highest oscillations with amplitudes of 7.5 cm occur in the head of the Gulf of Finland, Gulf of Bothnia, and in the Kalmar Strait.

In baroclinic conditions, high-frequency free oscillations (periods of 13, 19, 23, 27, and 41 h) are also observed. However, their role is minor, with amplitudes that are significantly lower than the amplitude of lower-frequency oscillations. In baroclinic conditions, oscillations of periods from several months to one year with total amplitudes reaching 15–17 cm, appear (fig.9). The area with the highest amplitudes of free baroclinic

451 oscillations is located in the deep part of the Baltic proper, where the highest gradients of water density are
452 observed (Terziev et al., 1992).

453
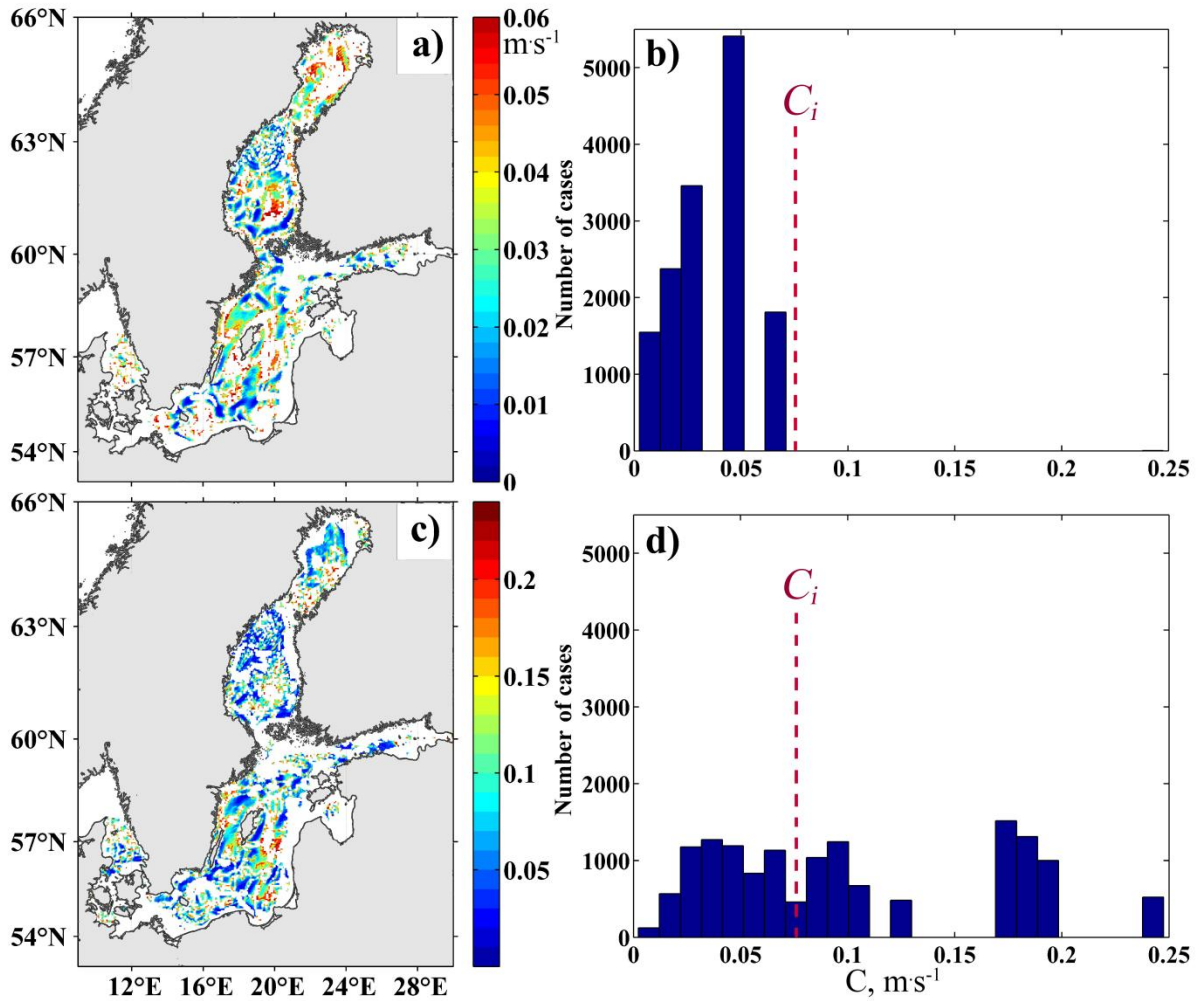
454
455 **Figure 15. Maps and histograms of phase speed (m s⁻¹) of progressive-standing waves of 385-day period (a,b) and 89-**
456 **day period (c,d). In the regions colored in white, the estimated phase speed equals to zero. Dash line on the histogram**
457 **plots indicates minimum value of theoretical phase speed of baroclinic gravity waves.**

458

459

460 Barotropic and baroclinic free-sea level oscillations with periods of 13–41 h represent multi-node progressive-
461 standing waves with amphidromic systems rotating in different directions. The speed of the isophase rotation in
462 barotropic amphidromic systems of 13 and 27 h periods is close to the theoretical phase speed of barotropic
463 gravity waves, while the phase speed of the amphidromic systems with a 41 h period is lower than that of gravity
464 waves. In baroclinic conditions, the values of progressive-standing wave phase speeds usually disagree with the
465 theoretical values of gravity wave phase speed estimated for stratified sea.
466 Correct identification of the described free barotropic and baroclinic oscillations in the Baltic Sea can help to
467 explain many large-scale variabilities of different physical characteristics (for example, large-scale sea level
468 changes).

469 According to theoretical investigations by LeBlond and Mysak (LeBlond and Mysak, 1978), a sea basin is

470 characterised by its own set of frequencies of barotropic and baroclinic oscillations. These oscillations refer to

471 two classes. The eigenoscillations of the first class are long gravity waves representing longitudinal waves. In

472 no-boundary ocean conditions and under the effect of the Earth's rotation, this type of wave is generated with

473 frequencies that are above the local inertial frequency. An introduction of a boundary results in trapping the

474 wave energy and generating trapped gravity Kelvin waves (Pedlosky, 1979). The Kelvin wave is the only wave

475 type existing in both band frequencies, above and below the inertial frequency (Pedlosky, 1979). Kelvin waves

476 always propagate anticlockwise in the Northern Hemisphere and clockwise in the Southern Hemisphere.

477 Eigenoscillations of the second class are planetary waves. Among them, Rossby and topographic waves have

478 been extensively investigated (LeBlond and Mysak, 1978). Rossby waves are horizontal transverse waves that

479 are generated in the frequency band, which are below inertia frequencies (Pedlosky, 1979). Rossby waves

480 always propagate westward, while topographic waves move along isobath lines and leave sharp bathymetry from

481 their right in the Northern Hemisphere and from their left in the Southern Hemisphere.

482 In semi-enclosed sea basins, the mechanism of wave reflection may have an significant effect on the propagation

483 of long waves and can lead to the generation of progressive-standing modes of gravity and planetary waves

484 (LeBlond and Mysak, 1978; Nekrasov, 1975; Pedlosky, 1979).

485 An earlier theoretical investigation of the dynamics of topographic Rossby waves in enclosed basins (Buchwald,

486 1973; LeBlond and Mysak, 1978; Pedlosky, 1979) demonstrated that they may have characteristics both standing

487 and progressive waves. Two types of node lines were observed in the (Longuet-Higgins, 1965) study during the

488 experiment in a rectangular basin: lines approximated by an envelope function with nodes stable in spatio-

489 temporal domain, as well as lines of progressive waves moving westward with a Rossby wave phase speed.

490 Theoretical studies of long gravity waves in enclosed or semi-enclosed basins that account for the Earth's

491 rotation have shown that these waves transform into multi-node progressive-standing Kelvin waves (Nekrasov,

492 1975; Pugh, 1987; Taylor, 1922). The overall effect of the Earth's rotation on free oscillations is to vitiate the

493 development of fixed nodal lines and to atrophy them into nodal points or amphidromic centres (Wilson B. W.,

494 1972). Then, an oscillation rotates around the amphidromic centre in the form of a Kelvin wave such that the

495 amplitude increases from zero in its centre to the maximum on basin boundaries. In the Northern Hemisphere,

496 this rotation is anticlockwise and changes to clockwise in the Southern Hemisphere.

497 Besides the Coriolis force, the opposite rotation of isophases in amphidromic systems may result from the

498 interference of standing waves (Harris, 1904; Nekrasov, 1975; Proudman, 1953; Schwiderski, 1979). Multiple

499 combinations of amplitude, angle, and phase differences of interfering waves are possible and may lead

500 anticlockwise to clockwise rotation.

501 The analysis of our numerical simulations coincides with the results of these theoretical experiments. The

502 opposite phase rotation is found for progressive-standing waves with a 27 h period (anticlockwise, similar to the

503 Kelvin wave) and for progressive-standing waves with 13 h and 41 h periods (clockwise). The comparison of the

504 phase speed of simulated free barotropic oscillations with theoretical values suggests that most of the oscillations

505 with periods of 13 h and 27 h are barotropic gravity waves. Other waves with 27 h periods and almost all waves

506 with 41 h periods are likely to be related to barotropic modes of topographic Rossby waves as their phase speed

507 is lower than that of the theoretical barotropic gravity waves, and their period is longer than that of inertial

508 oscillations (about 14 h).

509   Compared with barotropic conditions, the number and location of amphidromic systems in a stratified sea

510   change remarkably (Fig. 7a and Fig. 12a). By their phase speed, most of the free oscillations in the baroclinic

511   conditions of high (13 h) and medium (27 h) frequencies, as well as a substantial portion of oscillations at a

512   lower frequency (41 h), can be identified as barotropic gravity waves.

513   Our experiments demonstrate that in a stratified sea, the percentage of relatively slow-moving free waves

514   significantly increases compared with an unstratified sea. These changes can be associated with the generation of

515   the baroclinic mode of the topographic Rossby waves in a stratified medium. The significant difference in the

516   phase pattern in baroclinic and barotropic conditions (see Section 3.2) can be explained by the superposition of

517   the phases of 1) barotropic gravity waves and 2) barotropic/baroclinic modes of the topographic Rossby waves.

518   We also noted that there is no evidence of the existence of the baroclinic mode of long gravity waves in the

519   Baltic Sea because most of our phase speed estimates for the 13 and 27 h oscillations do not agree with the range

520   of theoretical phase speeds of the internal gravity waves estimated for local baroclinic conditions.

521   Free sea level oscillations at seasonal scales (periods of 3 months to 1 year) have a baroclinic origin, as they

522   appear only in baroclinic simulations. Maximal amplitudes of free oscillations of the 358-day and 89-day periods

523   do not exceed 2.5-5.5 cm (fig.14). These amplitudes are of the same order as the amplitudes of annual Baltic Sea

524   level variability (4 - 13 cm) estimated using stationary approximation from the tide gauges (Ekman, 1996;

525   Medvedev, 2014). The phase speed of the oscillations in the 358-day period is lower than the theoretical values

526   for the internal gravity waves and significantly varies from the range of values typical for barotropic gravity

527   waves. We relate these oscillations to the baroclinic mode of topographic Rossby waves. A fraction of waves of

528   the 89-day period is also the topographic Rossby waves. However, the other part of these oscillations has phase

529   speeds ($0.01–0.24$ m s^{-1}) overlapping with the range of theoretical values of the internal gravity waves ($0.08–$

530   1.53 m s^{-1}). This part can be identified as a baroclinic gravity wave.

531   Several studies have demonstrated that amplitudes of seasonal fluctuations in the Baltic sea level have important

532   inter-annual variability(Barbosa and Donner, 2016; Cheng et al., 2018; Ekman, 1998; Samuelsson and

533   Stigebrandt, 1996; Stramska et al., 2013). Considering that the free oscillations of seasonal-scale frequencies

534   have a baroclinic origin, we hypothesise that they could contribute to the non-stationary nature of these seasonal

535   fluctuations. Major Baltic Inflows (MBIs) are well-known sporadic events that import saline waters into the

536   Baltic. In recent decades, their occurrence has changed significantly (Fischer and Matthäus, 1996; Matthäus,

537   2006). The MBI events, along with the inter-annual variability of the freshwater input via atmospheric

538   precipitation and river flow affect the Baltic Sea water mass stratification (Assessment of Climate, 2008). The

539   inter-annual variability in the stratification, in turn, may affect the frequencies of the baroclinic modes of the

540   Baltic Sea eigenoscillations. As a result, from year to year, the resonance of atmospheric forces with the

541   baroclinic modes of free sea level oscillations can occur at different seasonal-scale frequencies or may not occur

542   at all. This mechanism may be one of the reasons responsible for the unsteady character of the Baltic sea level

543   seasonal variability and its role will be studied in the future.

544

545

546

547

548

Conclusion

The results of our numerical simulations of the free sea level oscillations of the Baltic Sea revealed a general similarity, with a distinct difference in the processes of relaxation of sea level oscillation in barotropic and baroclinic conditions.

1. The predominant common feature is the generation of oscillations in the same mesoscale frequency range (13–41 h) in both the unstratified and stratified sea experiments. These oscillations have the form of one- or multi-node progressive-standing waves with amphidromic systems rotating in opposite directions depending on the oscillation period.

2. The primary difference between the results of the experiments consists in the generation of sea level baroclinic oscillations of seasonal scales with periods of 89 and 358 days in stratified sea.

3. The highest amplitudes of free barotropic oscillations occur in the eastern part of the Gulf of Finland, in the Gulf of Bothnia, in the south-western Baltic proper, and in the Kalmar Strait. The highest amplitudes of baroclinic oscillations are found in the deep areas with the highest stratification of water masses in the Baltic proper.

4. Free barotropic oscillations of periods of 13 h and 27 h represent long gravity waves. Most of the 41 h period barotropic oscillations are likely to be the barotropic mode of the topographic Rossby wave.

5. The essential part of free oscillations of 13–41 h periods in the baroclinic conditions may be regarded as topographic Rossby waves generated in semi-enclosed basins. However, there is a minor part of these oscillations that may represent barotropic gravity waves. We did not find evidence of the existence of the baroclinic mode of long gravity waves at these frequencies.

6. Regarding free oscillations at a seasonal scale, we suggest that all oscillations of 358 days and half of the oscillations of 89 days are related to the baroclinic mode of the topographic Rossby waves, as their phase speeds do not overlap with the theoretical values estimated for internal gravity waves. However, the other part of 89-day baroclinic oscillations, with their phase speed, is likely to be the baroclinic gravity waves.

Based on the results of our numerical experiments, we can conclude that after the cessation of the atmospheric forcing, the relaxation of the Baltic free sea level oscillations occurs in the form of barotropic and baroclinic modes of progressive-standing gravity waves as well as in the form of topographic Rossby waves. The free baroclinic oscillations contribute significantly to the spectre of the Baltic Sea eigenoscillations. Their role is the most important in seasonal-scale sea level fluctuations.

Acknowledgements. This research was made possible with support from the Saint-Petersburg University, Grant № IAS_18.37.140.2014. The authors express their gratitude towards Dr. A.Kouraev (Toulouse University) for his valuable support and suggestions.

References

Barbosa, S. M. and Donner, R. V.: Long-term changes in the seasonality of Baltic sea level, Tellus, Ser. A Dyn. Meteorol. Oceanogr., 68(1), doi:10.3402/tellusa.v68.30540, 2016.

Berrisford, P., Dee, D., Fielding, K., Fuentes, M., Kallberg, P., Kobayashi, S. and Uppala, S.: The ERA-Interim Archive - Version 2.0., 2011.

Briegleb, B., Bitz, C., Hunke, E., Lipscomb, W., Holland, M., Schramm, J. and Moritz, R.: Scientific description of the sea ice component in the Community Climate System Model, Boulder, Colorado., 2004.

Brydon, D., Sun, S. and Bleck, R.: A new approximation of the equation of state for seawater, suitable for numerical ocean models, J. Geophys. Res. Ocean., 104(C1), doi:10.1029/1998jc900059, 1999.

Buchwald, V. T.: Long period divergent planetary waves, Geophys. Fluid Dyn., 5(1), doi:10.1080/03091927308236125, 1973.

Carmack, E. C. and Kulikov, E. A.: Wind-forced upwelling and internal Kelvin wave generation in Mackenzie Canyon, Beaufort Sea, J. Geophys. Res. Ocean., 103(C9), doi:10.1029/98JC00113, 1998.

Cheng, Y., Xu, Q. and Li, X.: Spatio-temporal variability of annual sea level cycle in the Baltic Sea, Remote Sens., 10(4), doi:10.3390/rs10040528, 2018.

Diansky, N. A.: Modeling of ocean circulation and study of its response to short-period and long-period atmospheric influences, PHYSMATLIT, Moscow., 2013.

Diansky, N. A., Zalesny, V. B., Moshonkin, S. N. and Rusakov, A. S.: High resolution modeling of the monsoon circulation in the Indian Ocean, Oceanology, 46(5), doi:10.1134/S000143700605002X, 2006.

Diansky, N. A., Panasenkova, I. and Fomin, V.: Investigation of the Barents Sea Upper Layer Response to the Polar Low in 1975, Phys. Oceanogr., 35(6), 467–483, doi:10.22449/1573-160x-2019-6-467-483, 2019.

Diansky, N. A., Stepanov, D. V., Fomin, V. V. and Chumakov, M. M.: Water Circulation Off the Northeastern Coast of Sakhalin during the Passage of Three Types of Deep Cyclones over the Sea of Okhotsk, Russ. Meteorol. Hydrol., 45(1), doi:10.3103/S1068373920010045, 2020.

Ekman, M.: A common pattern for interannual and periodical sea level variations in the Baltic Sea and adjacent waters, Geophysica, 32(3), 1996.

Ekman, M.: Secular change of the seasonal sea level variation in the Baltic Sea and secular change of the winter climate, Geophysica, 34(3), 1998.

Fennel, W. and Seifert, T.: Oceanographic processes in the Baltic Sea, Kuste, (74), 2008.

Fischer, H. and Matthäus, W.: The importance of the Drogden Sill in the Sound for major Baltic inflows, J. Mar. Syst., 9(3–4), doi:10.1016/S0924-7963(96)00046-2, 1996.

Fomin, V. V. and Diansky, N. A.: Simulation of Extreme Surges in the Taganrog Bay with Atmosphere and Ocean Circulation Models, Russ. Meteorol. Hydrol., 43(12), doi:10.3103/S1068373918120051, 2018.

Guide: Guide to Marine Hydrological Forecasts, Hydrometeoizdat, Sankt-Petersburg., 1994.

Harris, R.: Manual of tides, Phys. Hydrogr., IV, 313–400, 1904.

Hunke, E. C. and Dukowicz, J. K.: An elastic-viscous-plastic model for sea ice dynamics, J. Phys. Oceanogr., 27(9), doi:10.1175/1520-0485(1997)027<1849:AEVPMF>2.0.CO;2, 1997.

Jönsson, B., Döös, K., Nycander, J. and Lundberg, P.: Standing waves in the Gulf of Finland and their relationship to the basin-wide Baltic seiches, J. Geophys. Res. Ocean., 113(3), doi:10.1029/2006JC003862, 2008.

Korshenko, E. A., Diansky, N. A. and Fomin, V. V.: Reconstruction of the black sea deep-water circulation using INMOM and comparison of the results with the ARGO buoys data, Phys. Oceanogr., 26(3), doi:10.22449/1573-160X-2019-3-202-213, 2019.

Kulikov, E. A. and Medvedev, I. P.: Variability of the Baltic Sea level and floods in the Gulf of Finland, Oceanology, 53(2), doi:10.1134/S0001437013020094, 2013.

LeBlond, P. and Mysak, L.: Waves in the Ocean, in Elsevier Oceanographi Series 20, p. 602, Elsever, Amsterda-Oxford-New York. [online] Available from: eLSEVER, 1978.

Leppäranta, M. and Myrberg, K.: Physical Oceanography of the Baltic Sea., 2009.

Lisitzin, E.: Uninodal Seiches in the Oscillation System Baltic proper-Gulf of Finland, Tellus, 11(4), doi:10.3402/tellusa.v11i4.9325, 1959.

Lisitzin, E.: Sea level changes, in Elsevier Oceanogr. Series, p. 286., 1974.

Longuet-Higgins, M.: Planetary waves on a rotating sphere. II, Proc. R. Soc. London. Ser. A. Math. Phys. Sci., 284(1396), 40–68, doi:10.1098/rspa.1965.0051, 1965.

Magaard, L. and Krauss, W.: Spektren der Wasserstandsschwankungen der Ostee im Jahre 1958, Kieler Meeresforschungen, 22, 155–162, 1966.

Matthäus, W.: The history of investigation of salt water inflows into the Baltic Sea - from the early beginning to recent results, Meereswissenschaftliche Berichte Mar. Sci. Reports, 65(65), 2006.

Medvedev, I. P.: Seasonal fluctuations of the Baltic Sea level, Russ. Meteorol. Hydrol., 39(12), doi:10.3103/S106837391412005X, 2014.

Metzner, M., Gade, M., Hennings, I. and Rabinovich, A. B.: The observation of seiches in the Baltic Sea using a multi data set of water levels, J. Mar. Syst., 24(1–2), doi:10.1016/S0924-7963(99)00079-2, 2000.

Morozov, E. G., Frey, D. I., Diansky, N. A. and Fomin, V. V.: Bottom circulation in the Norwegian Sea, Russ. J. Earth Sci., 19(2), doi:10.2205/2019ES000655, 2019.

Moshonkin, S., Zalesny, V. and Gusev, A.: Simulation of the Arctic-North Atlantic Ocean circulation with a two-equation K-omega turbulence parameterization, J. Mar. Sci. Eng., 6(3), doi:10.3390/JMSE6030095, 2018.

Nekrasov, A.: Tidal waves in marginal seas, Hydrometeoizdat, Leningrad., 1975.

Neumann, G.: Eigenschwigungen der Ostsee, Arch. Dtsch. Hambg., 61, 4–59, 1941.

653   Pedlosky, J.: Geophysical fluid dynamics, Springer-Verlag, New York. [online] Available from:
654   https://www.academia.edu/9388448/Geophysical_Fluid_Dynamics_Joseph_Pedlosky, 1979.
655   Proshutinsky, A.: Fluctuations of the water level of the Arctic Ocean, Hydrometeoizdat, Sankt-Petersburg., 1993.
656   Proudman, J.: Dynamical Oceanography, Methuen and Co, London., 1953.
657   Pugh, D. T.: Tides, Surges and Mean Sea-Level, Natural Environment Research Council Swindon., 1987.
658   Samuelsson, M. and Stigebrandt, A.: Main characteristics of the long-term sea level variability in the Baltic sea,
659   Tellus, Ser. A Dyn. Meteorol. Oceanogr., 48(5), doi:10.3402/tellusa.v48i5.12165, 1996.
660   Schwiderski, E.: Global ocean tides. Part II. The semidiurnal principal lunar tide 884 (M2)., 1979.
661   Stramska, M., Kowalewska-Kalkowska, H. and Świrgoń, M.: Seasonal variability in the Baltic Sea level,
662   Oceanologia, 55(4), doi:10.5697/oc.55-4.787, 2013.
663   Taylor, G. I.: Tidal oscillations in gulfs and rectangular basins, Proc. London Math. Soc., s2-20(1),
664   doi:10.1112/plms/s2-20.1.148, 1922.
665   Terziev, F., Rozhkov, V. and Smirnova, A., Eds.: Hydrometeorology and hydrochemistry of the Seas of the
666   USSR. The Baltic Sea, Gidrometeoizdat, Sankt-Petersburg., 1992.
667   Voynov, G.: Tidal phenomena and the methodology of their research in the shelf zone of the Arctic seas, Sankt-
668   Petersburg., 2003.
669   Wilson B. W.: Seiches, Adv. Hydrosci., 1, 1–89, 1972.
670   Wübber, C. and Krauss, W.: The two-dimensional seiches of the Baltic Sea, Oceanol. Acta, 4(2), 1979.
671   Yakovlev, N.: Reconstruction of the large-scale state of waters and sea ice cover of the Arctic Ocean as of 1948-
672   2002 years. Part 1: Numerical model and average state., Phisical Ocean Atmos., 45(3), 1–16, 2009.
673   Zakharchuk, E. A. and Tikhonova, N. A.: On the spatiotemporal structure and mechanisms of the Neva River
674   flood formation, Russ. Meteorol. Hydrol., 36(8), doi:10.3103/S106837391108005X, 2011.
675   Zakharchuk, E. A., Tikhonova, N. A. and Fuks, V. R.: Free low-frequency waves in the Baltic Sea, Russ.
676   Meteorol. Hydrol., (11), 2004.
677   Zalesny, V. B., Diansky, N. A., Fomin, V. V., Moshonkin, S. N. and Demyshev, S. G.: Numerical model of the
678   circulation of the Black Sea and the Sea of Azov, Russ. J. Numer. Anal. Math. Model., 27(1), doi:10.1515/rnam-
679   2012-0006, 2012.